one of the crucial residues mediating such a pH-dependent conformational change.

Experimental procedures

Materials

Succinimidyl-6-(biotinamide)hexanoate (NHS-LC-biotin) and streptavidin-conjugated agarose were purchased from Pierce Chemicals (Rockford, IL). The amiloride derivative EIPA was a gift from New Drug Research Laboratories of Kanebo, Ltd (Osaka, Japan). ^{22}NaCl was purchased from Dupont NEN (Boston, MA). All other chemicals used were of the highest purity available.

Cells, culture conditions, and stable expression

An Na^+/H^+ exchanger-deficient cell line (PS120) [21] and the corresponding transfectants were maintained in DMEM (Sigma-Aldrich, St Louis, MO) containing 25 mM $NaHCO_3$ and supplemented with 7.5% (v/v) fetal bovine serum, penicillin (50 U·mL^{-1}), and streptomycin (50 μg·mL^{-1}) at 37 °C in the presence of 5% CO_2. The PS120 cells (5×10^5 cells per 100 mm dish) were transfected with each plasmid construct (10 μg) by using the calcium phosphate coprecipitation technique. Cell populations that stably expressed mutant NHE1 were selected by the 'H^+-killing' technique, as described previously [23].

Construction of NHE mutants

A plasmid carrying cDNA coding for the NHE1 human isoform and containing some unique restriction sites that was cloned into the pECE mammalian expression vector was described previously [23]. We used a PCR-based strategy to construct point-mutant cDNA, as described previously [22], by using a template plasmid coding for the HA-tagged wild-type NHE1 [12]. The DNA sequences of the PCR fragments were confirmed using an Applied Biosystems (Tokyo, Japan) Model 3130 autosequencer.

Surface biotinylation and immunoblot analysis

Confluent cells cultured on 60 mm dishes were washed twice with 5 mL of NaCl/P_i containing 0.1 mM $CaCl_2$ and 1 mM $MgCl_2$ (NaCl/P_iCM, pH 7.2) and were subsequently incubated in 1 mL of NaCl/P_iCM containing 1 mM NHS-LC-biotin for 30 min at room temperature. After the cells had been washed twice with 5 mL of NaCl/P_iCM, they were solubilized with 1 mL of lysis buffer containing 1% Triton X-100, 150 mM NaCl, 20 mM Hepes/Tris (pH 7.4), 1 mM phenylmethanesulfonyl fluoride, and 1 mM benzamidine. After centrifugation for 10 min at 16 000 *g* (RT15A3 rotor, Hitachi himac CF15D microcentrifuge), the supernatant was mixed with streptavidin-agarose beads (30 μL of resin) and incubated for 1 h at 4 °C with mild agitation. After centrifugation as described above, the unbound and total proteins were separated on a 3–8% gel by SDS/PAGE and analyzed by immunoblotting with an antibody against the HA tag, as described previously [23]. The blots were developed using an enhanced chemiluminescence detection system (GE Healthcare, Chalfont St Giles, UK). The protein bands were densitometrically scanned using IMAGEJ version 1.37I imaging software (NIH, Bethesda, MD).

Measurement of $^{22}Na^+$ uptake

The $^{22}Na^+$-uptake activity and its pH_i dependence were measured by the K^+/nigericin pH_i clamp method [15]. Cells in 24-well plates were serum-depleted for more than 5 h and preincubated for 30 min at 37 °C in Na^+-free choline chloride/KCl medium containing 20 mM Hepes/Tris (pH 7.4), 1.2–140 mM KCl, 2 mM $CaCl_2$, 1 mM $MgCl_2$, 5 mM glucose, and 5 μM nigericin. Next, $^{22}Na^+$ uptake was initiated by adding the same choline chloride/KCl solution containing ^{22}NaCl (37 kBq·mL^{-1}) (final concentration, 1 mM), 1 mM ouabain, and 100 μM bumetanide. In some wells, the uptake solution contained 0.1 mM EIPA. Furthermore, in some experiments, the uptake solutions containing various concentrations of Na^+, Li^+, or EIPA were adjusted to various pH values. After 1 min of Na^+ uptake, the cells were rapidly washed four times with ice-cold NaCl/P_i to terminate the reaction. The pH_i was calculated on the basis of the imposed $[K^+]$ gradient by assuming the equilibrium $[K^+]_i/[K^+]_o = [H^+]_i/[H^+]_o$ and an intracellular $[K^+]$ of 120 mM. The data obtained were normalized with regard to protein concentration, which was measured using the bicinchoninic assay system (Pierce Chemicals) with BSA as the standard.

Measurement of pH_i

The change in pH_i induced by various extracellular agents was measured by the [^{14}C]benzoic acid equilibration method, as described previously [23].

Statistics

Data regarding the pH dependence of $^{22}Na^+$ uptake were simulated by fitting the values to the sigmoidal dose–response equation, i.e. rate of EIPA-sensitive $^{22}Na^+$ uptake = $V_{max}/(1 + 10^{\wedge}[\log(pK - pH_i)^n])$ (pK, pH_i considering half-maximal $^{22}Na^+$ uptake; n, Hill coefficient), using a simulation program included in the graphing software PRISM (v. 4.0c, GraphPad Software Inc., San Diego, CA). The dependence of the $^{22}Na^+$ uptake on the extracellular Na^+ concentration was fitted to the steady-state kinetic

equation by using the same simulation program, and dependencies on extracellular Li^+, pH and EIPA were fitted to the one-site competition equation. The kinetic parameters were expressed as the best fitted values with standard errors, and the other data were expressed as the means ± SD for at least three determinations.

Acknowledgements

We thank Dr K. Naruse, Dr S. Mohri (Okayama University), and Dr H. Suga (National Cardiovascular Center Research Institute) for giving us the opportunity to collaborate with an excellent trainee (Mr K. Yamada). We also thank Ms M. Miyazaki for technical assistance. This work was supported by a Grant-in-Aid for Priority Areas 18077015 and 18059035 for Scientific Research from the Ministry of Education, Science and Culture of Japan, by Grant for Cardiovascular Diseases (17A-1) from the Ministry of Health, Labor, Welfare of Japan, and by the Program for Promotion of Fundamental Studies in Health Science of the National Institute of Biomedical Innovation (NIBIO), and in part the Salt Science Research Foundation (No.0737) and Health, Labor Sciences Research Grants.

References

1 Wakabayashi S, Shigekawa M & Pouysségur J (1997) Molecular physiology of vertebrate Na^+/H^+ exchangers. *Physiol Rev* **77**, 51–74.
2 Orlowski J & Grinstein S (2004) Diversity of the mammalian sodium/proton exchanger SLC9 gene family. *Pflugers Arch* **447**, 549–565.
3 Counillon L & Pouysségur J (2000) The expanding family of eucaryotic Na^+/H^+ exchangers. *J Biol Chem* **275**, 1–4.
4 Putney LK, Denker SP & Barber DL (2002) The changing face of the Na^+/H^+ exchanger, NHE1: structure, regulation, and cellular actions. *Annu Rev Pharmacol Toxicol* **42**, 527–552.
5 Slepkov E & Fliegel L (2002) Structure and function of the NHE1 isoform of the Na^+/H^+ exchanger. *Biochem Cell Biol* **80**, 499–508.
6 Zachos NC, Tse M & Donowitz M (2005) Molecular physiology of intestinal Na^+/H^+ exchange. *Annu Rev Physiol* **67**, 411–443.
7 Karmazyn M, Sostaric JV & Gan XT (2001) The myocardial Na^+/H^+ exchanger: a potential therapeutic target for the prevention of myocardial ischaemic and reperfusion injury and attenuation of postinfarction heart failure. *Drugs* **61**, 375–389.
8 Engelhardt S, Hein L, Keller U, Klambt K & Lohse MJ (2002) Inhibition of Na^+-H^+ exchange prevents hypertrophy, fibrosis, and heart failure in β_1-adrenergic receptor transgenic mice. *Circ Res* **90**, 814–819.
9 Aronson PS, Nee J & Suhm MA (1982) Modifier role of internal H^+ in activating the Na^+-H^+ exchanger in renal microvillus membrane vesicles. *Nature* **299**, 161–163.
10 Aronson PS (1985) Kinetic properties of the plasma membrane Na^+-H^+ exchanger. *Annu Rev Physiol* **47**, 545–560.
11 Wakabayashi S, Hisamitsu T, Pang T & Shigekawa M (2003) Kinetic dissection of two distinct proton binding sites in Na^+/H^+ exchangers by measurement of reverse mode reaction. *J Biol Chem* **278**, 43580–43585.
12 Hisamitsu T, Pang T, Shigekawa M & Wakabayashi S (2004) Dimeric interaction between the cytoplasmic domains of the Na^+/H^+ exchanger NHE1 revealed by symmetrical intermolecular cross-linking and selective co-immunoprecipitation. *Biochemistry* **43**, 11135–11143.
13 Fafournoux P, Noël J & Pouysségur J (1994) Evidence that Na^+/H^+ exchanger isoforms NHE1 and NHE3 exist as stable dimers in membranes with a high degree of specificity for homodimers. *J Biol Chem* **269**, 2589–2596.
14 Hisamitsu T, Ben Ammar Y, Nakamura TY & Wakabayashi S (2006) Dimerization is crucial for the function of the Na^+/H^+ exchanger NHE1. *Biochemistry* **45**, 13346–13355.
15 Ikeda T, Schmitt B, Pouysségur J, Wakabayashi S & Shigekawa M (1997) Identification of cytoplasmic subdomains that control pH-sensing of the Na^+/H^+ exchanger (NHE1): pH-maintenance, ATP-sensitive, and flexible loop domains. *J Biochem (Tokyo)* **121**, 295–303.
16 Pang T, Hisamitsu T, Mori H, Shigekawa M & Wakabayashi S (2004) Role of calcineurin B homologous protein in pH regulation by the Na^+/H^+ exchanger 1: tightly bound Ca^{2+} ions as important structural elements. *Biochemistry* **43**, 3628–3636.
17 Pang T, Su X, Wakabayashi S & Shigekawa M (2001) Calcineurin homologous protein as an essential cofactor for Na^+/H^+ exchangers. *J Biol Chem* **276**, 17367–17372.
18 Ben Ammar Y, Takeda S, Hisamitsu T, Mori H & Wakabayashi S (2006) Crystal structure of CHP2 complexed with NHE1-cytosolic region and an implication for pH regulation. *EMBO J* **25**, 2315–2325.
19 Wakabayashi S, Hisamitsu T, Pang T & Shigekawa M (2003) Mutations of Arg440 and Gly455/Gly456 oppositely change pH sensing of Na^+/H^+ exchanger 1. *J Biol Chem* **278**, 11828–11835.
20 Lacroix J, Poet M, Maehrel C & Counillon L (2004) A mechanism for the activation of the Na/H exchanger NHE-1 by cytoplasmic acidification and mitogens. *EMBO Rep* **5**, 91–96.
21 Pouysségur J, Sardet C, Franchi A, L'Allemain G & Paris S (1984) A specific mutation abolishing Na^+/H^+

antiport activity in hamster fibroblasts precludes growth at neutral and acidic pH. *Proc Natl Acad Sci USA* **81**, 4833–4837.
22 Wakabayashi S, Pang T, Su X & Shigekawa M (2000) A novel topology model of the human Na^+/H^+ exchanger isoform 1. *J Biol Chem* **275**, 7942–7949.
23 Wakabayashi S, Fafournoux P, Sardet C & Pouysségur J (1992) The Na^+/H^+ antiporter cytoplasmic domain mediates growth factor signals and controls 'H^+-sensing'. *Proc Natl Acad Sci USA* **89**, 2424–2428.
24 Alexander RT, Malevanets A, Durkan AM, Kocinsky HS, Aronson PS, Orlowski J & Grinstein S (2007) Membrane curvature alters the activation kinetics of the epithelial Na^+/H^+ exchanger, NHE3. *J Biol Chem* **282**, 7376–7384.
25 Hayashi H, Szászi K, Coady-Osberg N, Orlowski J, Kinsella JL & Grinstein S (2002) A slow pH-dependent conformational transition underlies a novel mode of activation of the epithelial Na^+/H^+ exchanger-3 isoform. *J Biol Chem* **277**, 11090–11096.
26 Gerchman Y, Olami Y, Rimon A, Taglicht D, Schuldiner S & Padan E (1993) Histidine-226 is part of the pH sensor of NhaA, a Na^+/H^+ antiporter in *Escherichia coli*. *Proc Natl Acad Sci USA* **90**, 1212–1216.
27 Rimon A, Gerchman Y, Olami Y, Schuldiner S & Padan E (1995) Replacements of histidine 226 of NhaA-Na^+/H^+ antiporter of *Escherichia coli*. Cysteine (H226C) or serine (H226S) retain both normal activity and pH sensitivity, aspartate (H226D) shifts the pH profile toward basic pH, and alanine (H226A) inactivates the carrier at all pH values. *J Biol Chem* **270**, 26813–26817.
28 Dibrov P, Young PG & Fliegel L (1998) Functional analysis of amino acid residues essential for activity in the Na^+/H^+ exchanger of fission yeast. *Biochemistry* **37**, 8282–8288.
29 Wiebe CA, Dibattista ER & Fliegel L (2001) Functional role of polar amino acid residues in Na^+/H^+ exchangers. *Biochem J* **357**, 1–10.
30 Cha B, Oh S, Shanmugaratnam J, Donowitz M & Yun CC (2003) Two histidine residues in the juxta-membrane cytoplasmic domain of Na^+/H^+ exchanger isoform 3 (NHE3) determine the set point. *J Membr Biol* **191**, 49–58.
31 Tsuboi Y, Inoue H, Nakamura N & Kanazawa H (2003) Identification of membrane domains of the Na^+/H^+ antiporter (NhaA) protein from Helicobacter pylori required for ion transport and pH sensing. *J Biol Chem* **278**, 21467–21473.
32 Olkhova E, Hunte C, Screpanti E, Padan E & Michel H (2006) Multiconformation continuum electrostatics analysis of the NhaA Na^+/H^+ antiporter of *Escherichia coli* with functional implications. *Proc Natl Acad Sci USA* **103**, 2629–2634.
33 Counillon L, Franchi A & Pouysségur J (1993) A point mutation of the Na^+/H^+ exchanger gene (NHE1) and amplification of the mutated allele confer amiloride resistance upon chronic acidosis. *Proc Natl Acad Sci USA* **90**, 4508–4512.
34 Counillon L, Noël J, Reithmeier RA & Pouysségur J (1997) Random mutagenesis reveals a novel site involved in inhibitor interaction within the fourth transmembrane segment of the Na^+/H^+ exchanger-1. *Biochemistry* **36**, 2951–2959.
35 Slepkov ER, Chow S, Lemieux MJ & Fliegel L (2004) Proline residues in transmembrane segment IV are critical for activity, expression and targeting of the Na^+/H^+ exchanger isoform 1. *Biochem J* **379**, 31–38.
36 Noël J, Germain D & Vadnais J (2003) Glutamate 346 of human Na^+-H^+ exchanger NHE1 is crucial for modulating both the affinity for Na^+ and the interaction with amiloride derivatives. *Biochemistry* **42**, 15361–15368.
37 Orlowski J & Kandasamy RA (1996) Delineation of transmembrane domains of the Na^+/H^+ exchanger that confer sensitivity to pharmacological antagonists. *J Biol Chem* **271**, 19922–19927.
38 Wang D, Balkovetz DF & Warnock DG (1995) Mutational analysis of transmembrane histidines in the amiloride-sensitive Na^+/H^+ exchanger. *Am J Physiol* **269**, C392–C402.
39 Khadilkar A, Iannuzzi P & Orlowski J (2001) Identification of sites in the second exomembrane loop and ninth transmembrane helix of the mammalian Na^+/H^+ exchanger important for drug recognition and cation translocation. *J Biol Chem* **276**, 43792–43800.
40 Slepkov ER, Rainey JK, Li X, Liu Y, Cheng FJ, Lindhout DA, Sykes BD & Fliegel L (2005) Structural and functional characterization of transmembrane segment IV of the NHE1 isoform of the Na^+/H^+ exchanger. *J Biol Chem* **280**, 17863–17872.
41 Vinothkumar KR, Smits SH & Kuhlbrandt W (2005) pH-induced structural change in a sodium/proton antiporter from Methanococcus jannaschii. *EMBO J* **24**, 2720–2729.
42 Hunte C, Screpanti E, Venturi M, Rimon A, Padan E & Michel H (2005) Structure of a Na^+/H^+ antiporter and insights into mechanism of action and regulation by pH. *Nature* **435**, 1197–1202.
43 Yamashita A, Singh SK, Kawate T, Jin Y & Gouaux E (2005) Crystal structure of a bacterial homologue of Na^+/Cl^- dependent neurotransmitter transporters. *Nature* **437**, 215–223.

The American Journal of Pathology, Vol. 171, No. 5, November 2007

DOI: 10.2353/ajpath.2007.070452

Musculoskeletal Pathology

Enhanced Na^+/H^+ Exchange Activity Contributes to the Pathogenesis of Muscular Dystrophy via Involvement of P2 Receptors

Yuko Iwata, Yuki Katanosaka, Takashi Hisamitsu, and Shigeo Wakabayashi

From the Department of Molecular Physiology, National Cardiovascular Center Research Institute, Osaka, Japan

A subset of muscular dystrophy is caused by genetic defects in dystrophin-associated glycoprotein complex. Using two animal models (BIO14.6 hamsters and *mdx* mice), we found that Na^+/H^+ exchanger (NHE) inhibitors prevented muscle degeneration. NHE activity was constitutively enhanced in BIO myotubes, as evidenced by the elevated intracellular pH and enhanced $^{22}Na^+$ influx, with activation of putative upstream kinases ERK42/44. NHE inhibitor significantly reduced the increases in baseline intracellular Ca^{2+} as well as Na^+ concentration and stretch-induced damage, suggesting that $Na^+{}_i$-dependent Ca^{2+} overload via the Na^+/Ca^{2+} exchanger may cause muscle damage. Furthermore, ATP was found to be released continuously from BIO myotubes in a manner further stimulated by stretching and that the P2 receptor antagonists reduce the enhanced NHE activity and dystrophic muscle damage. These observations suggest that autocrine ATP release may be primarily involved in genesis of abnormal ionic homeostasis in dystrophic muscles and that Na^+-dependent ion exchangers play a critical pathological role in muscular dystrophy. *(Am J Pathol 2007, 171:1576–1587; DOI: 10.2353/ajpath.2007.070452)*

Muscular dystrophy is a heterogeneous genetic disease that causes severe skeletal muscle degeneration, characterized by fiber weakness and muscle fibrosis. The genetic defects associated with muscular dystrophy often include mutations in one of the components of the dystrophin-glycoprotein complex, such as dystrophin or sarcoglycans (α-, β-, γ-, and δ-SG).[1–3] The dystrophin-glycoprotein complex is a multisubunit complex[2,4,5] that spans the sarcolemma to form a structural link between the extracellular matrix and the actin cytoskeleton.[6] Disruption of dystrophin-glycoprotein complex significantly impairs membrane integrity or stability during muscle contraction/relaxation and prevents myocyte survival. This enhanced susceptibility to exercise-induced damage of muscle fibers is observed in dystrophic animals, such as δ-SG-deficient BIO14.6 hamsters and dystrophin-deficient *mdx* mice, genetic homologues of human limb-girdle and Duchenne muscular dystrophy, respectively.

Despite identification of many genes responsible for muscular dystrophy, the pathways through which genetic defects lead to muscle dysgenesis are still poorly understood. Myocyte degeneration has long been attributed to membrane defects, such as increased fragility to mechanical stress. Enhanced membrane stretching results in increased permeability to Ca^{2+}, and the resultant abnormal Ca^{2+} handling has been suggested to be a prerequisite for muscle dysgenesis. A number of studies have indicated chronic elevation in the cytosolic Ca^{2+} concentration ($[Ca^{2+}]_i$), beneath the sarcolemma, or within other cell compartments in skeletal muscle fibers or in cultured myotubes from dystrophin-deficient (Duchenne muscular dystrophy) patients and *mdx* mice.[7–9] Recently, we identified one of the stretch-activated channels, the growth factor responsive channel (GRC, TRPV2), which may be involved in the pathogenesis of myocyte degeneration caused by dystrophin-glycoprotein complex disruption.[10] More recently, we found that Ca^{2+}-handling drugs, such as tranilast and diltiazem, exert protective effects against muscle degeneration in

Supported by the Ministry of Education, Culture, Sports, Science, and Technology of Japan (grant-in-aid for priority areas 18077015, grants-in-aid 16590726 and 17659241, and a grant for the Cooperative Link for Unique Science and Technology for Economy Revitalization); the Ministry of Health, Labor, and Welfare (Promotion of Fundamental Studies in Health Sciences of National Institute of Biomedical Innovation, research grants for cardiovascular diseases no. 17A-1, and for nervous and mental disorders no. 16B-2); and the Salt Science Research Foundation (grant 0539).

Accepted for publication July 24, 2007.

Supplemental material for this article can be found on *http://ajp.amjpathol.org*.

Address reprint requests to Yuko Iwata or Shigeo Wakabayashi, Department of Molecular Physiology, National Cardiovascular Center Research Institute, Fujishiro-dai 5-7, Suita, Osaka 565 Japan. E-mail: wak@ri.ncvc.go.jp.

both *mdx* mice and BIO14.6 hamsters,[11] suggesting that Ca^{2+}-permeable channels primarily contribute to abnormal Ca^{2+}-homeostasis in dystrophic animals. In addition to the Ca^{2+}-entry pathway across the plasma membrane, it is also plausible that modifications of other ion-transport proteins contribute to genesis of the abnormal Ca^{2+} homeostasis in muscular dystrophy. We discovered that plasma membrane Na^+/H^+ exchanger (NHE) inhibitors are highly protective against muscle damage in dystrophic animals. NHE is an important transporter regulating the intracellular pH (pH_i), Na^+ concentration ($[Na^+]_i$), and cell volume, and catalyzing the electroneutral countertransport of Na^+ and H^+ through the plasma membrane or organelle membranes.[12–14] The housekeeping isoform, NHE1, is activated rapidly in response to various extracellular stimuli, such as hormones, growth factors, and mechanical stressors.[12] Enhanced NHE activity would cause elevation of $[Na^+]_i$ and may produce intracellular Ca^{2+} overload via reduced Ca^{2+} extrusion by the plasma membrane Na^+/Ca^{2+} exchanger (NCX). Although Ca^{2+} overload caused by Na^+-dependent ion exchangers has been studied extensively in ischemic hearts,[15–17] such phenomena have not been reported in dystrophic skeletal muscles. The protective effects of NHE inhibitors suggest that in addition to the Ca^{2+}-permeable channel(s), Na^+-dependent ion exchangers may be involved in the pathogenesis of muscular dystrophy, presumably through the sustained increase in $[Ca^{2+}]_i$.

Here, we first show that the NHE inhibitors, cariporide and 5-(*N*-ethyl-*N*-isopropyl)-amiloride (EIPA), have protective effects against muscle degeneration in dystrophic BIO14.6 hamsters and *mdx* mice. We also show that the NHE activity is constitutively enhanced in dystrophic myotubes and that cariporide significantly reduces both the elevated $[Na^+]_i$ and $[Ca^{2+}]_i$. Furthermore, we show that P2 receptor stimulation with ATP released by stretching may be the mechanism underlying the constitutive activation of NHE. To our knowledge, this is the first report indicating the pathological importance of Na^+-dependent ion exchangers in muscular dystrophy.

Materials and Methods

Materials

Cariporide was a gift from Aventis Pharma Chem. Ltd. (Frankfurt, Germany), and EIPA and KB-R7943(KBR) were from the New Drug Research Laboratories of Kanebo, Ltd. (Osaka, Japan). Rabbit polyclonal antibodies against NHE1 and NCX1 were described previously.[18–20] Rabbit polyclonal antibody against p44/42 MAP kinase and mouse monoclonal antibody against phospho-p44/42 MAP kinase (T202/Y204) were purchased from Cell Signaling (Beverly, MA). Gadolinium chloride ($GdCl_3$) hexahydrate, ouabain, apyrase, 6-azaophenyl-2′,4′-disulfonic acid (PPADS), suramin, and monensin were purchased from Sigma Chemical (St. Louis, MO). Thapsigargin was from Calbiochem (La Jolla, CA). $^{22}NaCl$ was purchased from NEN Life Science Products (Boston, MA). Fura-2/acetoxymethylester (AM) and fluo4-AM were from Dojindo Laboratories (Tokyo, Japan) and Molecular Probes (Eugene, OR), respectively.

Animal Experiments

Our study followed institutional guidelines of National Cardiovascular Center for animal experimentation and was performed under the approved protocol. For examination of drug effects, EIPA and cariporide were administered orally in either the drinking water at a drug/body weight ratio of 3 mg/kg per day to 60-day-old BIO14.6 hamsters or 50-day-old *mdx* mice or age-matched normal controls as described.[21] Suramin was administered by intraperitoneal injection at 25 mg/kg per day.[22] After continuous administration for periods indicated in legends to each figure, animals were subjected to measurement of creatine phosphokinase (CK) level in serum, histochemical analysis of muscles, and grip test. For the grip test for *mdx* mice, forelimb grip strength of *mdx* mice was assessed by timing how long they could support their body weight by holding onto a fine wire net. Each group consisted of more than five mice, all of which were analyzed twice on 2 different days.

Histochemical Analysis of Muscles

Skeletal muscles were fixed in phosphate-buffered saline (PBS) containing 10% formalin and embedded in paraffin. Serial 5-μm sections were stained with hematoxylin and eosin (H&E) or Masson's trichrome. The extent of experienced damage occurring in muscles was determined by comparing the number of centrally located nuclei between samples using a light microscopy. Variability of fiber size was obtained by averaging the standard deviations from three to four cross-sectional views of myofibers from three to four animals per group. The extent of fibrosis (blue-staining area) was measured on photographs of Masson's trichrome-stained sections.

Culture of Myotubes

Myotubes in culture were prepared as described previously.[10,11] In brief, myoblast cells were isolated from the gastrocnemius muscles of normal or BIO14.6 hamsters by enzymatic dissociation. Minced muscles (0.3 g) were incubated for 45 minutes at 37°C in 1 ml of Ham's F-12 medium containing 2 U/ml dispase and 1% collagenase. After filtration through a fine mesh nylon filter and preplating to remove fibroblasts, cells were plated with ~80% confluence onto collagen I-coated culture dishes in growth medium consisting of Ham's F-12 medium supplemented with 20% fetal calf serum and 2.5 ng/ml basic fibroblast growth factor (Promega BRL, Madison, WI) and 1% chick embryo extract (Life Technologies, Inc., Grand Island, NY). One or 2 days after plating, medium was changed to Dulbecco's modified Eagle's medium containing 2% horse serum (Hyclone Laboratories, Logan, UT) to initiate differentiation. Myoblasts begin to fuse and form myotubes in culture within 24 hours. We used the myotubes 2 to 5 days after the switch to differentiation medium.

Measurement of $^{22}Na^+$ Uptake

Normal and BIO14.6 myotubes cultured on collagen I-coated silicon membranes or in 24-well dishes were incubated at 37°C for 30 minutes in uptake solution containing 50 mmol/L NaCl, 96 mmol/L choline chloride, 1 mmol/L $MgCl_2$, 0.1 mmol/L $CaCl_2$, 10 mmol/L glucose, 0.1% bovine serum albumin, 10 mmol/L HEPES/Tris, pH 7.4, 37 kBq/ml $^{22}NaCl$, and 1 mmol/L ouabain. In some wells, the uptake solution contained 0.1 mmol/L EIPA or/and 0.25 mmol/L $GaCl_3$. After 30 minutes, cells were rapidly washed four times with ice-cold PBS to terminate $^{22}Na^+$ uptake. Cells were lysed in 0.1 N NaOH, and aliquots were taken for determination of protein and radioactivity.

Measurement of pH_i and $[Na^+]_i$

Myoblasts from skeletal muscles were seeded onto 25-mm glass coverslips coated with collagen I (Becton, Dickinson and Company, Franklin Lakes, NJ) and differentiated into myotubes. Myotubes were loaded with 3 μmol/L 2′,7′-bis-(bis-(2-carboxyethyl)-5(6)-carboxyfluorescein acetoxymethyl ester (BCECF-AM) in balanced salt solution (BSS) (146 mmol/L NaCl, 4 mmol/L KCl, 2 mmol/L $MgCl_2$, 1 mmol/L $CaCl_2$, 10 mmol/L glucose, 0.1% bovine serum albumin, and 10 mmol/L HEPES/Tris, pH 7.4) for 10 minutes at room temperature. The coverslip was mounted on a flow chamber and continuously perfused with solutions at 0.6 ml/minute with a Perista pump. Changes in intracellular pH (pH_i) were estimated by ratiometric scanning of changes in BCECF fluorescence. Fluorescence was monitored by alternatively exciting at 440 and 490 nm through a 505-nm dichroic reflector and 510- to 530-nm band-path emission filter. Fluorescence images were collected every 10 seconds using a cooled charge-coupled device camera (ORCA-ER; Hamamatsu Photonics, Hamamatsu, Japan) mounted onto an inverted microscope (IX 71; Olympus, Tokyo, Japan) with a ×20 objective (UApo/340; Olympus) and were then processed with AQUACOSMOS software (Hamamatsu Photonics). The pH_i value was calibrated with high K^+ solution containing 5 μmol/L nigericin adjusted to various pH values. For measurement of $[Na^+]_i$, myotubes were incubated with 10 μmol/L sodium-binding benzofuran isophthalate acetoxymethyl ester (SBFI-AM) and Pluronic F-127 (0.05% w/v) in BSS for 120 minutes at room temperature. After washout, SBFI-AM was de-esterified for 20 minutes. SBFI fluorescence was monitored by alternatively exciting at 340 and 380 nm at 1 Hz through a 505-nm dichroic reflector and 510- to 530-nm band-path emission filter. In some experiments we used BSS buffered with 10 mmol/L $NaHCO_3$ (pH 7.4), saturated with 5% CO_2 and 95% O_2 gas. Fluorescence images were collected as described above for pH_i measurement. The fluorescence ratio at 340:380 was calculated with AQUACOSMOS software and $[Na^+]_i$ was calibrated at the end of each experiment in solutions containing 0, 10, or 20 mmol/L extracellular NaCl in the presence of 10 μmol/L gramicidin, 1 mmol/L ouabain, and 2 μmol/L monensin.

Measurement of $[Ca^{2+}]_i$

For Ca^{2+} imaging, cells were plated on glass and cultured and loaded with fluo-4 by incubation for 30 minutes at 37°C in 4 μmol/L acetoxymethyl ester (Molecular Probes) in BSS as described previously.[10] In brief, fluorescence signals in cells were detected by confocal laser-scanning microscopy using a MRC-1024ES system (Bio-Rad, Richmond, CA) mounted on an Olympus BX50WI microscope with a ×60 water immersion lens. The frequency of image acquisition was selected as one image per <1 second. Analysis of single-frame or single-cell integrated signal density was performed with LaserSharp software (Bio-Rad, Hertfordshire, UK). The Ca^{2+} level was represented as ΔF/Fo, where Fo is the resting fluo-4 fluorescence and ΔF is the difference between peak steady-state fluorescence within 1 to 2 minutes after stimulation and resting fluorescence. In some experiments, we also loaded cells with 4 μmol/L fura-2 acetoxymethyl ester as described above and measured $[Ca^{2+}]_i$ by a ratiometric fluorescence method using a fluorescence image processor (Aquacosmos; Hamamatsu Photonics). The excitation wavelength was alternated at 340 and 380 (1 Hz), and we measured the fluorescence light emitted at 510 nm. The fluorescence ratio at 340:380 was calculated.

Application of Cell-Stretch to Myotubes in a Silicone Chamber

Mechanical stretching was applied to myotubes using a silicon chamber as described previously.[10] After cells were allowed to attach to the chamber bottom, uniaxial sinusoidal stretching was applied to the chamber at a constant strength from 5 to 20% elongation at 1 Hz for indicated periods. The relative elongation of the silicone membrane was uniform across the whole membrane area.

CK Activity and ATP Assay

After stretching of myotubes, CK activity in the medium was determined using an *in vitro* colorimetric assay kit (CK test kit; Wako Pure Chem. Co., Osaka, Japan) according to the protocol provided by the manufacturer. For ATP measurement, myotubes were washed twice with 0.5 ml of BSS 1 hour before stretching. BSS (0.5 ml) was added to the chamber, and uniaxial sinusoidal stretching was applied as above. Aliquots (100 μl) of the BSS solution were taken at selected times to measure the ATP level. The concentration of ATP released from the myotubes was measured using the luciferin-luciferase reaction (ENLITEN; Promega).

Other Procedures

Quantitative immunoblotting analysis and immunocytochemistry were performed as described previously.[10,11,23,24] Protein concentration was measured using a bicinchoninic acid assay system (Pierce Chemical Co., Rockford, IL) with bovine serum albumin as a standard. Unless

otherwise stated, experiments were performed at 25 ± 1°C and data are represented as means ± SD of at least three determinations. We used unpaired *t*-test, one-way analysis of variance followed by Dunnett's test, or two-way analysis of variance for statistical analyses. Values of $P < 0.05$ were considered statistically significant.

Results

NHE Inhibitors Prevent Skeletal Muscle Dysfunction and Cell Damage in Dystrophic Hamsters and Mice

Oral EIPA protected against muscle degeneration, as shown in sections stained with H&E (Figure 1A). We measured the number of fibers with central nuclei, which was often used as an index for regeneration to compensate for the fiber breakdown. The number of centrally localized nuclei was markedly reduced by treatment with EIPA (Figure 1Ba) or cariporide (see Figure 8, B and C). Among several other abnormal morphological features, dystrophic muscle fibers are known to display greater variations in their cross-sectional area because muscles contain fibers with different sizes, such as necrotic, splitting, and regenerating fibers. EIPA markedly reduced this fiber size variability as determined by the SD of the cross-sectional areas of myofibers (Figure 1Bb). In addition, NHE inhibitor considerably reduced the area of fibrosis stained with Masson's trichrome (see Figure 8Cb). These results suggest that NHE inhibitor prevented muscle degeneration and blocked the resultant regeneration as evidenced by the reduced centrally located nuclei. Furthermore, EIPA markedly reduced CK level in the serum of BIO14.6 hamsters, which is also a marker for muscle degeneration (Figure 1C). In *mdx* mice, the extent of muscle degeneration reaches the first peak in ~21 to 28 days and then declines because of regeneration and reaches the second peak in ~72 days, when muscle degeneration was checked by serum CK level. Therefore, we started the treatment with cariporide in 50-day-old mice to see whether muscle damage during the second period is reduced. As shown in Figure 1D, treatment with cariporide for 22 days (Figure 1Db) markedly prevented muscle damage. Cariporide reduced inflammatory infiltrate (Figure 1D), fibrosis (data not shown, but see Figure 8), and the number of myofibers with central nuclei particularly in mice treated for 60 days (Figure 1E). In control *mdx* mice, serum CK levels reached a peak in 72 days of age (22 days after start of experiment) and remained at relatively high level until 145 days of age (95 days after start of experiment, Figure 1F). Treatment with cariporide considerably reduced serum CK level in all investigated ages in *mdx* mice (Figure 1F). Together, these results suggest that the degenerative and accompanying regenerative episodes become rare on treatment with NHE inhibitor. Furthermore, we also evaluated the muscle performance of mice by timing how long they could support their body weight holding onto a fine wire net. Cariporide significantly improved the results of this grip test in *mdx* mice (Figure 1G). These observations collectively suggest that inhibition of NHE activity confers a significant protective effect against skeletal muscle dysfunction in dystrophic animals.

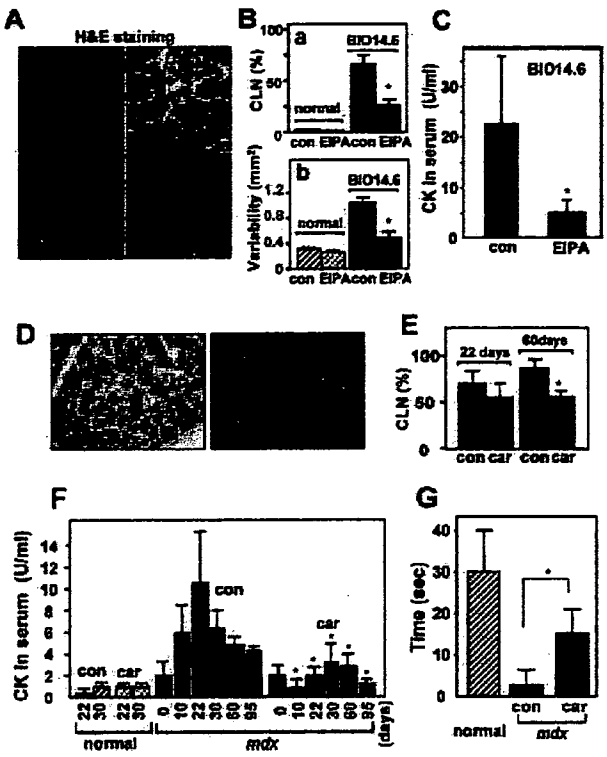

Figure 1. NHE inhibitors protect against muscle degeneration in dystrophic muscle. **A:** Histological staining of skeletal muscles. Gastrocnemius muscles were taken from normal (**a** and **c**) or BIO14.6 (**b** and **d**) hamsters administered with EIPA (**c** and **d**) or no EIPA (**a** and **b**) for 14 days and sections were stained with hematoxylin (red) and eosin (blue). EIPA was administered orally to 60-day-old BIO14.6 hamsters up to 74 days. **B:** Quantitation of fibers containing central nuclei in the gastrocnemius muscles of normal and BIO14.6 hamsters administered with EIPA or no EIPA (con). Centrally located nuclei (**a**) and variability in fiber size (**b**) were measured as described in Materials and Methods. Data are means ± SD (n = 3 to 4). $^*P < 0.05$ versus BIO14.6/control. **C:** Effect of EIPA on CK level in serum from BIO14.6 hamsters. Data are means ± SD (n = 5). $^*P < 0.05$. In normal hamsters, the serum CK level was less than 0.3 U/ml. **D:** H&E staining of muscle sections from *mdx* mice administered with cariporide (**b**) for 22 days and age-matched (72-day-old) control *mdx* mice (**a**). **E:** Quantitation of fibers containing central nuclei in the muscle sections from *mdx* mice administered with cariporide (car) or no drug (con) for 22 or 60 days. **F:** Effect of cariporide on serum CK level in normal and *mdx* mice. Drug administration was started in 50-day-old mice (treatment, 0 day) and continued up to 145 days (treatment, 95 days). Data are means ± SD (n = 5), $^*P < 0.05$. **G:** Effect of cariporide on muscle performance measured with grip test. Cariporide-treated (car) for 22 days or control mice (con) gripped a wire mesh with their forefeet and the time until they let go was measured. Data are means ± SD (n = 5). $^*P < 0.05$. It is not statistically significant between normal and *mdx*/cariporide. Scale bars = 100 μm.

Enhanced Na^+/H^+ Exchange and Extracellular Signal-Regulated Kinases Activities in Myotubes from Dystrophic Hamsters

Our *in vivo* data prompted us to study the mechanism of the involvement of NHE in skeletal muscle dysgenesis. Immunoblotting analysis revealed that skeletal muscles expressed NHE1, and its expression level was not very different between skeletal muscles from normal and BIO14.6 hamsters (Figure 2A); the normalized relative

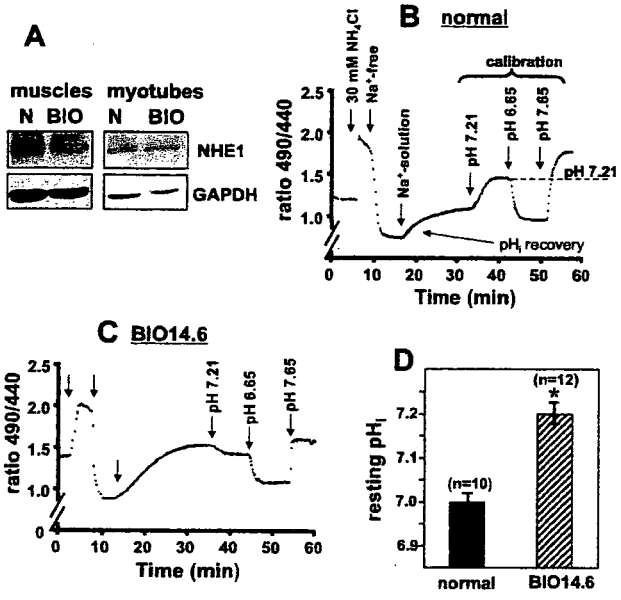

Figure 2. NHE1 expression and intracellular pH in normal and BIO14.6 myotubes. **A:** Immunoblotting analysis of NHE1 in normal and BIO14.6 hamster skeletal muscles and their cultured myotubes. Skeletal muscle (40 μg each) and myotube (10 μg each) homogenates were subjected to SDS-PAGE followed by immunoblotting analysis using the indicated antibodies. **B** and **C:** Typical traces of change in BCECF fluorescence intensity indicated as the ratio of excitation wavelength 490:440 in a single myotube from normal or BIO14.6 hamsters. Cells were acidified by NH_4^+ prepulse and then pH_i recovery was started by switching to Na^+-containing solution. To calibrate pH_i, cells were perfused with high K^+ solution containing 5 μmol/L nigericin adjusted to various pH values. **D:** Summarized data for resting level of pH_i. Data are means ± SD (n = 10 to 12). $^*P < 0.05$.

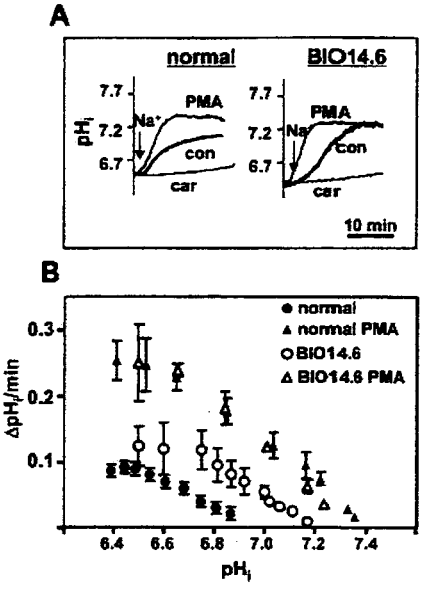

Figure 3. High Na^+/H^+ exchange activity in BIO14.6 myotubes. **A:** Time courses of Na^+-induced pH_i recovery in normal and BIO14.6 myotubes. Myotubes were subjected to NH_4^+ prepulse, and then pH_i recovery was induced by exposing myotubes to Na^+-containing solution. In some experiments, myotubes were exposed to 1 μmol/L PMA or 10 μmol/L cariporide throughout the NH_4^+ prepulse and pH_i recovery phases. **B:** The pH_i dependence of the pH_i recovery rates. The pH_i recovery rate was calculated from the increment in pH_i every 10 seconds and plotted against pH_i. Data are means ± SD of five independent experiments.

amount of NHE1 in BIO14.6 was 0.92 ± 0.07 (n = 3) versus normal muscles. NHE1 is distributed mainly in the sarcolemma of the skeletal muscles from normal and dystrophic hamsters (Supplemental Figure 1; see *http://ajp.amjpathol.org*). Moreover, we did not detect a large difference in the expression level (Figure 2A; 0.95 ± 0.08 versus normal myotubes, n = 3) of NHE1 between cultured myotubes from normal and BIO14.6 hamsters. We next measured the NHE activity after NH_4^+ prepulse by ratiometric fluorescence measurement with BCECF. In normal myotubes after NH_4^+ prepulse, the addition of external Na^+ induced rapid pH_i recovery, reaching only pH_i ~7.0 (Figure 2B). This pH_i recovery was attributable to the NHE activity because it was blocked completely by cariporide (Figure 3A). Because half-maximal inhibition occurred at relatively low cariporide concentration (<1 μmol/L), the NHE1 isoform was thought to be mainly involved in pH_i recovery. In contrast, in BIO14.6 myotubes pH_i recovered toward the higher pH_i range (>7.2) (Figure 2C). Myotubes from BIO14.6 hamsters exhibited significantly higher resting pH_i compared with normal animals (Figure 2D). Interestingly, although the PKC activator PMA markedly accelerated the pH_i recovery in normal myotubes, PMA accelerated only the initial pH_i recovery phase in BIO14.6 myotubes (Figure 3A). Figure 3B shows the pH_i dependence of pH_i recovery rate measured in myotubes. The pH_i dependence was shifted to the alkaline side in BIO14.6 as compared with normal myotubes. In normal myotubes, PMA greatly shifted the pH_i dependence to the alkaline side. In contrast in BIO14.6 myotubes, PMA did not induce a large alkaline shift of pH_i dependence although it elevated the recovery rate at each pH_i. These observations may reflect the high levels of activated NHE in BIO14.6 myotubes, inducing an alkaline shift of pH_i dependence resulting in a marginal effect of PMA.

The above findings suggest that some signaling pathways are constitutively activated and lead to the enhanced NHE activity in dystrophic myotubes. We examined the activity of extracellular signal-regulated kinases (ERKs) (ERK42/44) because ERKs were previously demonstrated to mediate the NHE activation in response to hormones or growth signals.[25–28] As shown in Figure 4, both PMA and mechanical stretch increased the level of phosphorylation of ERKs in normal myotubes (approximately three to four times). In contrast, phosphorylation of ERKs was high in BIO14.6 myotubes, even in the absence of extrinsic stimuli, and PMA and stretch did not further increase ERKs phosphorylation (Figure 4, A and B). These results suggest that ERKs are already activated in BIO14.6 myotubes.

Involvement of NHE in $[Na^+]_i$ and $[Ca^{2+}]_i$ Abnormalities in Dystrophic Myotubes

We next measured EIPA-inhibitable $^{22}Na^+$ uptake into myotubes, another index for the NHE activity. In normal myotubes, EIPA inhibited $^{22}Na^+$ uptake by more than 60%, whereas gadolinium ions (Gd^{3+}), which inhibit cation channels, inhibited it by only ~25%, indicating that NHE is one of the major Na^+ influx pathways in skeletal myotubes (Figure 5A). The EIPA-sensitive $^{22}Na^+$ uptake

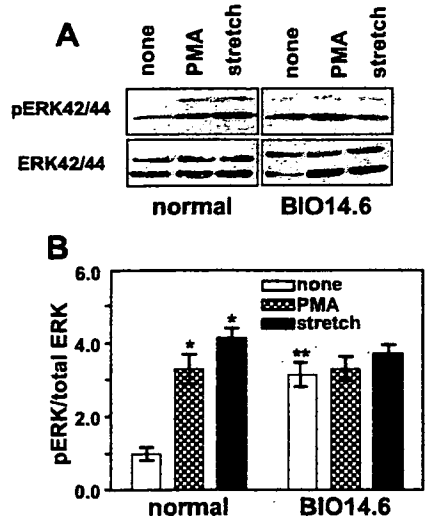

Figure 4. ERK42/44 is constitutively phosphorylated in BIO14.6 myotubes. **A:** Immunoblotting analysis of total and phosphorylated ERK42/44 in normal and BIO14.6 myotubes. Serum-starved (16 hours) myotubes were treated for 30 minutes with 1 μmol/L PMA or subjected to 20% elongation for 5 minutes (stretch). Myotubes were homogenized and then subjected to SDS-PAGE (10 μg each) followed by immunoblotting analysis with anti-phospho-ERK42/44 or anti-ERK42/44. **B:** The apparent amount of phosphorylated ERK42/44 was normalized relative to that of total ERK. Data are means ± SD of three independent experiments. $^*P < 0.05$ versus control, and $^{**}P < 0.05$ versus untreated control normal myotubes.

was higher (~1.5-fold) in BIO14.6 compared with normal myotubes (Figure 5B), consistent with the data for pH_i recovery. We measured the resting level of $[Na^+]_i$ in myotubes by means of ratiometric imaging technique with SBFI fluorescence in the absence or presence of bicarbonate. Consistent with the elevated $^{22}Na^+$ uptake

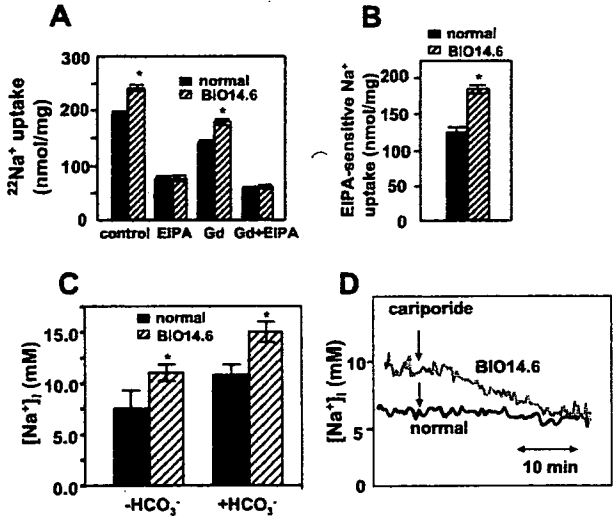

Figure 5. $^{22}Na^+$ uptake activity and intracellular Na^+ concentration. **A:** $^{22}Na^+$ uptake by myotubes was measured for 30 minutes as described in Materials and Methods. As indicated, 0.1 mmol/L EIPA or 0.25 mmol/L $GdCl_3$ was included in the $^{22}Na^+$ uptake solution. Data are means ± SD of triplicate determinations. $^*P < 0.05$ versus normal myotubes. **B:** EIPA-sensitive $^{22}Na^+$ uptake. $^*P < 0.05$. **C:** The resting level of $[Na^+]_i$ was measured using the SBFI fluorescence in the absence or presence of bicarbonate. For the latter experiment, BSS contained 10 mmol/L $NaHCO_3$ (pH 7.4) and bubbled for 30 minutes with 5% CO_2 and 95% O_2 immediately before the experiment. Means ± SD ($n = 3$). $^*P < 0.05$. **D:** Effect of cariporide on $[Na^+]_i$. At the time points indicated, myotubes were exposed to 10 μmol/L cariporide.

activity, BIO14.6 myotubes had significantly elevated resting $[Na^+]_i$ in the presence or absence of bicarbonate, when compared with wild-type myotubes, with the highest $[Na^+]_i$ in the presence of bicarbonate (Figure 5C). Treatment with cariporide caused a gradual reduction in $[Na^+]_i$ down to the control level (Figure 5D). These observations suggest that in addition to the resting pH_i, the enhanced Na^+/H^+ exchange activity causes elevation in $[Na^+]_i$ in BIO14.6 myotubes.

Elevated $[Na^+]_i$ may cause intracellular Ca^{2+} overload by altering the activity of sarcolemmal NCX. Therefore,

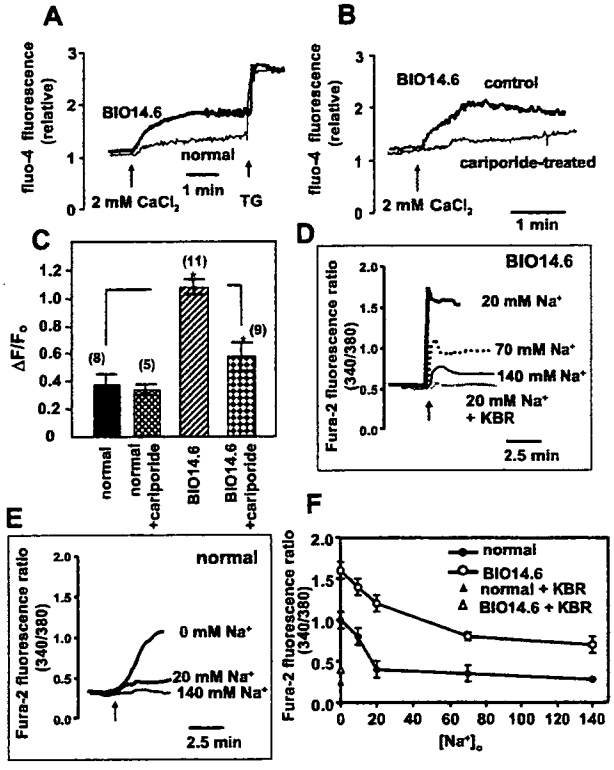

Figure 6. Effect of cariporide on intracellular Ca^{2+} increment and abnormal NCX function in BIO14.6 myotubes. **A:** Typical trace of changes in fluo-4 fluorescence intensity observed by confocal microscopy in normal or BIO14.6 myotubes loaded with fluo-4. The addition of 2 mmol/L $CaCl_2$ (final 2.5 mmol/L) to BSS containing 0.5 mmol/L $CaCl_2$ induced a marked increase in fluo-4 fluorescence in BIO14.6 myotubes. As indicated, exposure to 10 μmol/L thapsigargin (TG) induced a large increase in fluo-4 fluorescence in both myotubes. **B:** Effects of cariporide on external Ca^{2+}-induced change in fluo-4 fluorescence in BIO14.6 myotubes. Myotubes were pretreated with 10 μmol/L cariporide. **C:** Extracellular Ca^{2+}-induced maximal increments of fluorescence in myotubes pretreated with or without cariporide ($\Delta F/F_o$ is the ratio between the fluorescence increment and the fluorescence before Ca^{2+} addition). Data are means ± SD (trial numbers are shown in parentheses). $^*P < 0.05$ (versus control for drug effect). **D** and **E:** Effect of external Na^+ concentration on $[Ca^{2+}]_i$. Extracellular Ca^{2+}-induced rise in fluorescence ratio (340/380) was monitored by the Fura-2 fluorescence in BIO14.6 and normal myotubes, respectively. BIO14.6 myotubes were placed in BSS containing 0.5 mmol/L $CaCl_2$ and then Ca^{2+} mobilization was triggered by perfusing with a solution containing 2 mmol/L $CaCl_2$ and different concentrations of NaCl. When NaCl concentration was reduced, NaCl was replaced with choline chloride (total concentration, 140 mmol/L). In one experiment, 10 μmol/L KBR was included in the solution. **F:** Extracellular Na^+ concentration dependence of Ca^{2+}-induced increase in fluorescence ratio (340/380). Myotubes were loaded with Fura-2, perfused with BSS containing 0.5 mmol/L $CaCl_2$, and then Ca^{2+} mobilization was triggered with BSS containing 2 mmol/L $CaCl_2$ and different concentrations of NaCl (see **D** and **E**). Peak amplitude of the relative fluorescence ratio (340/380) was plotted against external Na^+ concentration. In some experiments, 10 μmol/L KBR was included in BSS. Data are means ± SD ($n = 3$).

we tested the effects of cariporide on $[Ca^{2+}]_i$. Figure 6A shows typical traces of extracellular Ca^{2+}-induced Ca^{2+} mobilization measured by fluo-4 fluorescence. The addition of 2 mmol/L $CaCl_2$ triggered a marked increase in $[Ca^{2+}]_i$ in BIO14.6 myotubes but very little change in normal myotubes, as described previously.[10,11] Pretreatment of BIO14.6 myotubes with 10 μmol/L cariporide for 30 minutes inhibited the Ca^{2+}-induced rise in $[Ca^{2+}]_i$ almost completely (Figure 6, B and C, for summary data). These results suggest that the Na^+/H^+ exchange activity contributes greatly to the increase in $[Ca^{2+}]_i$ observed in BIO14.6 myotubes. To test the possible involvement of NCX, we examined the effect of reduced Na^+ concentration on the Ca^{2+}-induced $[Ca^{2+}]_i$ rise. Exposure of myotubes to solutions with low Na^+ concentrations (20 or 70 mmol/L) induced larger $[Ca^{2+}]_i$ increases than normal Na^+ solution (140 mmol/L NaCl). (Figure 6D). In contrast, exposure of normal myotubes to 20 mmol/L Na^+ had only a marginal effect on $[Ca^{2+}]_i$, whereas exposure to the nominally Na^+-free solution resulted in a large $[Ca^{2+}]_i$ increase (Figure 6E). The peak $[Ca^{2+}]_i$ amplitude was plotted against external Na^+ concentration (Figure 6F). The $[Ca^{2+}]_i$ amplitude was highly Na^+-sensitive particularly in BIO14.6 myotubes. Decrease in the Na^+ concentration leads to the reduced transmembrane Na^+ gradient, which in turn causes increased Ca^{2+} influx via the reverse reaction of NCX. In fact, $[Ca^{2+}]_i$ rise in the low Na^+ solution was mostly inhibited by the NCX inhibitor KBR (Figure 6, D and F), which was reported to inhibit the reverse mode of NCX.[29] These findings suggest that the NCX contributes to increased $[Ca^{2+}]_i$ in BIO14.6 myotubes, which is at least partly caused by enhanced $[Na^+]_i$.

Furthermore, we also examined the effects of NHE inhibitors on stretch-induced release of CK, which is a marker of muscle damage. The application of cyclic stretching up to 20% elongation for 1 hour induced CK release from BIO14.6 myotubes (Supplemental Figure 2, control; see *http://ajp.amjpathol.org*). Treatment of myotubes with 10 μmol/L EIPA or 0.1 to 10 μmol/L cariporide 30 minutes before the stretch significantly reduced the CK release (~30 to 40%) (Supplemental Figure 2; see *http://ajp.amjpathol.org*, see also Figure 7F), suggesting that NHE inhibitors are capable of reducing the stretch-induced muscle damage. Thus, increased susceptibility of BIO14.6 myotubes to mechanical stretching may result from the $[Ca^{2+}]_i$ rise, which would be at least partly caused by the $[Na^+]_i$ increase via enhanced NHE activity.

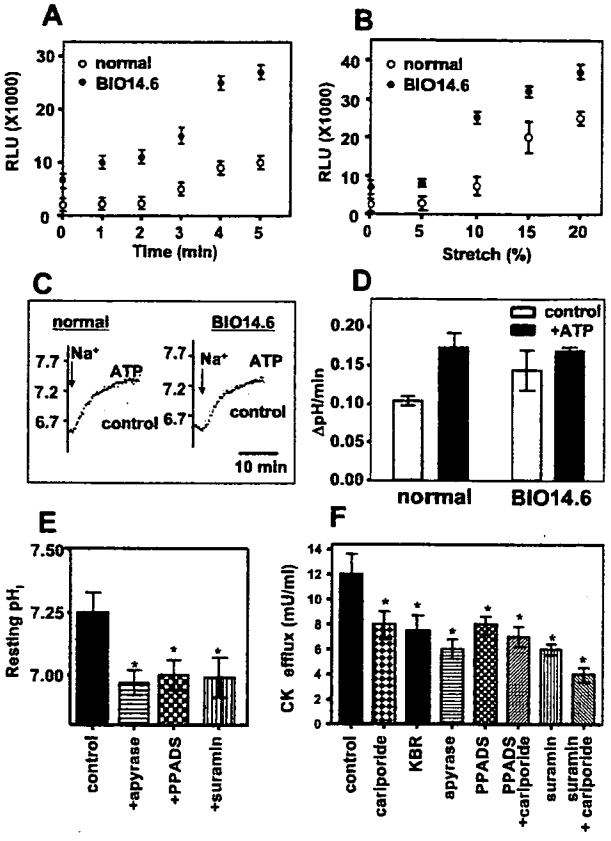

Figure 7. Enhanced ATP release from BIO14.6 myotubes and effect of ATP on normal and BIO14.6 myotubes. **A:** ATP release from elongated myotubes. Normal and BIO14.6 myotubes were subjected to cyclic 10% elongation for indicated periods in BSS. An aliquot of the supernatant was taken, and ATP concentration was measured with a luciferase-based luminescence kit as described in Materials and Methods. Data are means ± SD ($n = 3$). **B:** Effects of stretch strength (0 to 20%) on ATP release. Medium ATP contents 5 minutes after stretching are indicated. **C:** Effects of ATP on Na^+-induced pH_i recovery. Myotubes were subjected to NH_4^+ prepulse followed by Na^+-induced pH_i recovery. As indicated, myotubes were continuously exposed to 300 μmol/L ATP throughout the experiment during NH_4^+ prepulse and pH_i recovery phases. **D:** Summary data for maximal pH_i recovery rates. Data are means ± SD of three determinations. **E:** Effects of some pharmacological agents on the resting level of pH_i. BIO14.6 myotubes were incubated for 1 hour in BSS with and without indicated each drug and pH_i was measured. Apyrase, 0.4 U/ml; PPADS, 50 μmol/L; suramin, 100 μmol/L. Data are means ± SD ($n = 4$). **F:** Effects of various pharmacological agents on CK release from BIO14.6 myotubes. Myotubes were subjected to cyclic 20% elongation for 1 hour. Myotubes were preincubated with each drug for 10 minutes before stretching. Data are means ± SD ($n = 3$). $^*P < 0.05$ (versus control). Cariporide, 10 μmol/L; KBR, 10 μmol/L; PPADS, 50 μmol/L; suramin, 100 μmol/L; and apyrase, 0.4 U/ml.

Enhanced ATP Release in Myotubes from Dystrophic Hamsters and Protective Effects of P2 Receptor Antagonists against Muscle Damage

Activation of NHE and ERK as we mentioned above would be caused directly or indirectly by increased mechanical stress in dystrophic muscles. One possible mechanism is that hormonal factors released by stretching may stimulate their specific receptors, which in turn results in activation of downstream targets. We focused on ATP release because the expression pattern of purinergic receptors was recently reported to be greatly changed during muscular dysgenesis.[30,31] We measured the level of ATP released from myotubes into the medium by the luciferin-luciferase assay system before and after mechanical stretching. Stretching induced significant ATP release in both normal and BIO14.6 myotubes (Figure 7, A and B). Interestingly, stretch-induced ATP release was significantly higher in BIO14.6 myotubes compared with those from normal controls, and the ATP level was already high in the medium of cultured BIO14.6 myotubes before the stretch (Figure 7, A and B).

Moreover, ATP was found to accelerate the pH_i recovery rate and increased the resting level of pH_i in normal myotubes but not in those from BIO14.6 (Figure 7, C and D). To test whether the NHE activation in BIO14.6 myotubes is mediated by the release of ATP, we examined effects of several pharmacological agents on the resting level of pH_i. Preincubation of BIO myotubes with ATP-hydrolyzing enzyme apyrase, P2X receptor antagonist pyridoxal-5'-phosphate-6-azo-phenyl-2,4-disulfonate (PPADS) or general P2 receptor antagonist suramin, reduced the elevated resting pH_i in BIO myotubes, suggesting that ATP is an important extracellular driver of constitutive activation of NHE1. As expected, these pharmacological agents significantly reduced the stretch-induced CK efflux from BIO14.6 myotubes as effectively as did cariporide. Simultaneous incubation of myotubes with suramin and cariporide exerted the most effective protection (Figure 7F).

Finally, we examined whether the putative P2 receptor antagonist, suramin, improves muscular dysgenesis in dystrophic animals *in vivo*. Intraperitoneal injection of suramin significantly reduced the serum CK level to a similar extent as oral intake of cariporide (Figure 8A) and muscle damage as evidenced by Masson's trichrome staining (Figure 8B) in BIO14.6 hamsters. Furthermore, simultaneous administration of cariporide and suramin reduced the CK level and fibrosis more extensively as well as other abnormal dystrophic features such as the number of fibers with central nuclei or fiber size variability (Figure 8, A–C). A similar protective effect of suramin was also observed in *mdx* mice, as evidenced by significant reduction of serum CK level (Figure 8D) and improvement of muscle performance measured by the grip test (Figure 8E), suggesting that suramin has a protective effect against muscle dysgenesis in these animals.

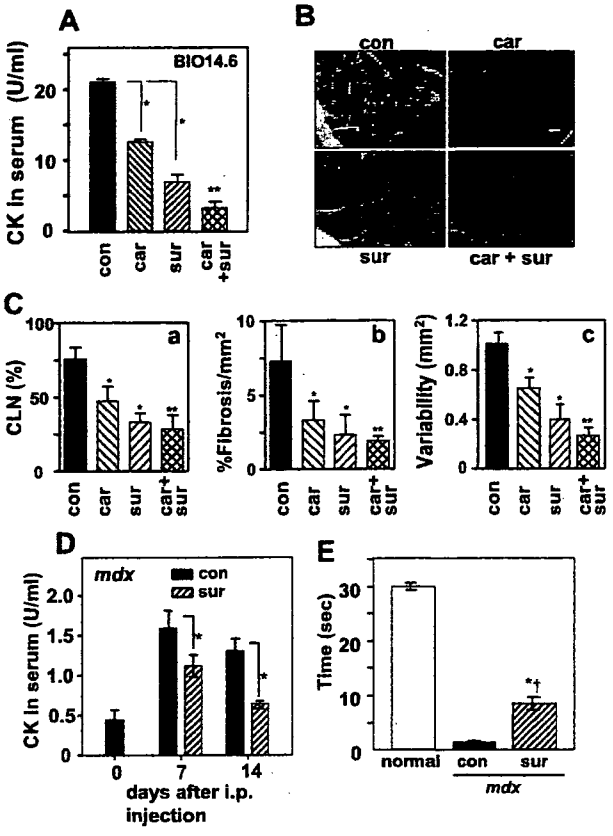

Figure 8. Protective effect of suramin against muscle degeneration. **A:** Effect of suramin and/or cariporide on CK level in serum from BIO14.6 hamsters. Suramin (sur) and/or cariporide (car) were administered by intraperitoneal injection or by oral intake into 60-day-old BIO14.6 hamsters, respectively, and 14 days after drug administration (74-day-old hamsters), serum CK level was measured. Data are means ± SD (n = 4 to 5). $^*P < 0.05$, whereas $^{**}P < 0.05$ versus either cariporide or suramin alone. **B:** Masson's trichrome staining of the quadriceps muscle sections from BIO14.6 hamsters. **C:** Quantitation of fibers containing central nuclei in muscles of BIO14.6 hamsters. Centrally located nuclei (**a**), fibrosis area (blue region) (**b**), and variability (**c**) were measured as described in Materials and Methods. Data are means ± SD (n = 3 to 4). $^*P < 0.05$. **D:** Effect of suramin on serum CK level in *mdx* mice. Suramin or PBS (for control) was injected into 14-day-old *mdx* mice and serum CK level was measured 7 or 14 days after the start of drug injection. **E:** Effect of suramin on muscle performance measured by the grip test. Data are means ± SD (n = 3 to 5). $^{*\dagger}P < 0.05$ versus *mdx*/control or normal/control, respectively. Scale bar = 100 μm.

Discussion

In the present study, we demonstrated that NHE inhibitors, cariporide and EIPA, have protective effects against muscle degeneration in dystrophic animals: BIO14.6 hamsters and *mdx* mice. NHE inhibitors significantly reduced the serum CK level, reduced the muscle damage, and improved the muscle performance measured by grip test. Furthermore, an *in vitro* study using cultured myotubes revealed that the NHE activity is constantly enhanced in myotubes from BIO14.6 hamsters, which would in turn contribute to the abnormal cytoplasmic Ca^{2+} handling, in part through inhibition of the Ca^{2+} extrusion by NCX or activation of the Ca^{2+} influx by reverse mode of NCX. Finally, we presented evidence that stimulation of P2 receptor with ATP released by stretching is a possible mechanism leading to activation of NHE. The results of the present study represent strong evidence that Na^+-dependent ion exchangers exert an important pathological impact on skeletal muscle degeneration caused primarily by genetic defects in cytoskeletal proteins. In Figure 9, we summarize a possible pathway leading to muscle degeneration, particularly based on the data from BIO14.6 hamsters. Although genetic background is different, we consider that a similar mechanism may be involved in the pathogenesis of BIO14.6 hamsters and *mdx* mice.

Until now, little attention has been paid to involvement of NHE in pathogenesis of muscular dystrophy. In this study, based on several criteria we found that NHE is constitutively activated in dystrophic BIO14.6 myotubes. The activity of NHE is known to be controlled by various extrinsic factors, including growth factors, hormones, and mechanical stimuli.[12,13] Although molecular mechanism of NHE activation is not well established, a large body of evidence suggested that both phosphorylation-dependent and -independent pathways are involved in the full activation of NHE1.[12] Hormones or growth factors bind to their specific receptors, which in turn stimulate the cell signaling pathways including PKC, G proteins, and various kinases, resulting in the activation of NHE. Indeed, the PKC activator PMA activated the pH_i recovery rate via

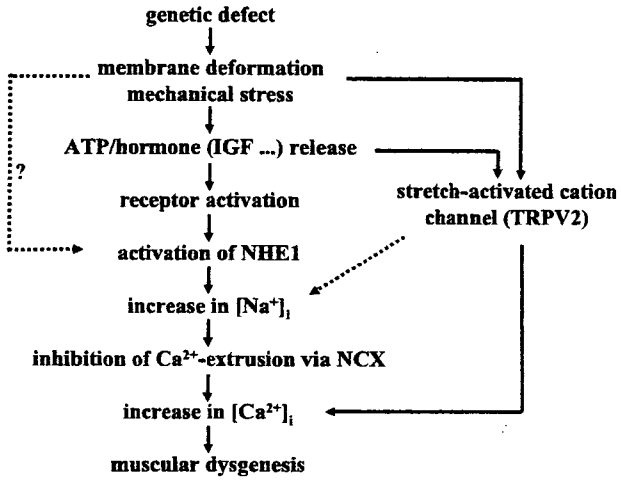

Figure 9. A possible pathway leading to muscle dysgenesis in BIO14.6 dystrophic hamsters suggested in this and previous studies.[10] A similar mechanism may underlie the pathogenesis of *mdx* mice.

a marked alkaline shift in the pH_i dependence in normal myotubes; however, in BIO14.6 myotubes the pH_i recovery rate was alkaline shifted even in the absence of PMA, suggesting that NHE is constitutively activated without externally added stimuli. This is compatible with the previous observation with ^{31}P-NMR that the resting muscle pH in *mdx* mice is more alkaline than that in normal muscle.[32] Previous studies reported that activation of ERK1/2 is a critical step in receptor-mediated stimulation of the exchanger in several cells.[25–28] In fact, this putative upstream kinase is phosphorylated in the resting state of BIO14.6 myotubes and is not further stimulated in response to PMA and stretch. This is compatible with recent studies to report that the phosphorylation of ERK1/2 is enhanced in dystrophic muscle fibers of *mdx* mice.[33,34]

Activation of NHE would result in accumulation of intracellular Na^+ as well as an increase in the resting pH_i, which would be pathologically important as a possible cause leading to muscle dysfunction. $[Na^+]_i$ is controlled by a balance between Na^+-extrusion via the Na^+ pump and Na^+ influx via multiple Na^+-coupled transporters and cation channels. Based on $^{22}Na^+$ flux experiments, we demonstrated that a major fraction (>60%) of Na^+ influx would be attributable to EIPA-sensitive Na^+/H^+ exchanger rather than Gd^{3+}-sensitive cation channels in myotubes from hamster skeletal muscles and $^{22}Na^+$ uptake via NHE is significantly higher in BIO14.6 myotubes. An increase in $[Na^+]_i$ has been reported previously in dystrophin-deficient *mdx* mice and eccentric stimulated muscle fibers.[35–37] In these previous studies, the $[Na^+]_i$ rise was suggested to be caused by either the reduced Na^+ pump activity[35,36] or the Gd^{3+}-inhibitable stretch-activated channel.[37] However, in contrast to these studies, our results suggest that NHE is the most likely candidate for the elevated $[Na^+]_i$, at least in BIO14.6 myotubes, although we cannot exclude the possibility of other Na^+-dependent pathways.

These observations raise the question of how the NHE inhibitors protect against muscle damage in dystrophic animals. Dystrophic damage has been thought to be attributable to the increase in $[Ca^{2+}]_i$. Elevated $[Ca^{2+}]_i$ would activate the Ca^{2+}-dependent protease calpain, which degrades various cellular proteins.[38] We demonstrated that BIO14.6 myotubes show abnormal cytosolic Ca^{2+} handling, as evidenced by the high resting $[Ca^{2+}]_i$ and frequently occurring Ca^{2+} oscillation.[10,11] These events have been attributed to the activation of stretch-activated nonspecific cation channels.[9,10,39] Importantly, preincubation with cariporide effectively reduced $[Ca^{2+}]_i$ and the level of CK released from BIO14.6 myotubes, suggesting that NHE, which is probably increased $[Na^+]_i$ via activated NHE, is involved in the genesis of abnormal Ca^{2+} homoeostasis. Furthermore, treatment with drugs that increase $[Na^+]_i$, monensin, significantly enhanced the stretch-induced CK release even in the normal myotubes (Supplemental Figure 2; see *http://ajp.amjpathol.org*), suggesting the pathological importance of intracellular Na^+. The increased $[Na^+]_i$ via NHE in muscles could lead to elevated $[Ca^{2+}]_i$ via either reduced Ca^{2+} extrusion or increased Ca^{2+} influx on NCX. Previous studies indicated that the NCX activity exists in skeletal muscle membranes[40] and contributes considerably to the regulation of $[Ca^{2+}]_i$ in muscle fibers.[41] By immunoblotting analysis, we also detected the existence of NCX1, amounts of which were similar in normal and BIO14.6 muscles (Supplemental Figure 1; see *http://ajp.amjpathol.org*). Exposure to the Na^+-reduced solution but containing millimolar concentrations of $CaCl_2$ induces a rapid increase in $[Ca^{2+}]_i$ and exerts severe damage on myotubes even in the absence of stretch, as evidenced by a massive increase in CK release (data not shown). The high Na^+ sensitivity of $[Ca^{2+}]_i$ and CK release imply the pathological importance of NCX in dystrophic damage. Given the resting membrane potential ~ -90 mV in skeletal muscle cells[42] and the reversal potential of NCX ~ -50 mV,[43] NCX is supposed to operate at the forward mode (Ca^{2+} extrusion) in normal and BIO14.6 myotubes. Therefore, increase in $[Na^+]_i$ would cause the elevation in $[Ca^{2+}]_i$ via reduced Ca^{2+} extrusion by NCX in the presence of normal external Na^+ concentration. However, long-chain fatty acyl CoA esters (acyl CoAs) were recently identified as endogenous regulatory factors that activate the reverse mode of NCX1,[44] suggesting that the reverse mode of NCX1 may be enhanced when the amount of acyl CoAs are elevated under pathological conditions. Acyl CoAs were reported to increase in muscles from patients with Duchenne dystrophy.[45] Thus, we do not exclude the possibility that increase in $[Na^+]_i$ might cause the elevation in $[Ca^{2+}]_i$ via enhanced Ca^{2+} influx by NCX in BIO14.6 myotubes.

It is an intriguing question which signaling pathway leads to activation of NHE. NHE is known to be activated in response to mechanical stressors, such as stretching, hyperosmotic, or shear stress.[12,46,47] It is possible that the NHE activity would increase as a result of autocrine/paracrine action of some hormones induced by stretching. In this study, we presented evidence that P2 receptor stimulation may be a likely mechanism leading to activation of NHE followed by muscle degeneration. We found that higher levels of ATP are released from BIO14.6 myo-

tubes in a stretch-dependent manner, which in turn would activate P2X or P2Y receptors via an autocrine mechanism. In both skeletal muscles and cultured myotubes, P2X2, P2X4, P2X7, and P2Y1 receptors were found to be expressed among P2X1, P2X2, P2X4, P2X7, P2Y1, and P2Y2 purinergic receptors tested by us by means of RT-PCR and immunoblot analysis, and these receptors are functional because ATP (and its analogues)-induced Ca^{2+} mobilization was observed and blocked by P2 antagonists in both myotubes (Y. Iwata, unpublished observations). ATP is considered one of the important nucleotides mediating its effect by activation of P2X and P2Y, which belong to the transmitter-gated cation channels and G protein-coupled receptors, respectively.[48] Recent studies demonstrated that ATP can regulate myoblast proliferation, differentiation, and regeneration *in vitro*[30] and that muscle cells of *mdx* mice show increased susceptibility to ATP.[31] Our data, together with these findings, suggest that ATP is one of the important mediators in the pathogenesis of dystrophic muscles. Although our data suggest the importance of P2 receptors, we think that our results should be evaluated with great caution because chemicals such as suramin and PPADS may also inhibit other target molecules. Besides ATP, we do not exclude the possibility that other factors are involved. Three growth factors have been so far reported to be related to muscular dystrophy: insulin-like growth factor-1 (IGF-1), fibroblastic growth factor, and transforming growth factor-β1.[49] These growth factors would also be important for dystrophic muscle pathology, because they are capable of activating NHE. For example, Perron and colleagues[50] reported that mechanical stretching induced autocrine secretion of IGF-1 in tissue cultures of differentiated avian pectoralis skeletal muscle cells. In our measurement, however, the IGF-1 concentration in serum was not as high in dystrophic animals (BIO14.6 hamsters and *mdx* mice) compared with normal animals, and in addition, scavenging of IGF-1 by anti-IGF-1 antibody did not block CK release in BIO14.6 myotubes (data not shown), suggesting that at least the contribution of IGF-1 may be rather small.

We found that ATP is released from BIO14.6 myotubes even in the absence of stimuli, and ATP concentration in the medium reached ~50 nmol/L after stretching. We also found that ATP concentration in the serum of dystrophic animals is significantly higher than that of normal controls (data not shown). In general, ATP concentration in the bulk medium is thought to be much lower than that localized close to the cell surface. For example, a previous study clearly showed that ATP levels in the proximity of the plasma membrane surface can be 10- to 20-fold higher than those in the bulk medium.[51] Recent experiments using the recombinant luciferase technique revealed that cells can release large amounts of ATP (100 to 200 μmol/L).[52] Therefore, it is likely that ATP exists in close proximity to the surface at concentrations sufficient for stimulation of P2 receptors, although further analyses are needed to determine the ATP concentration in the vicinity of the cell surface. ATP release has been reported to occur through several pathways, including exocytotic vesicles,[53] anion channels,[54,55] hemi-gap channels,[56,57] and some types of transporter.[58,59] It is possible that some of these pathways are activated by stretching in dystrophic muscles thereby resulting in enhanced release of ATP. In addition, because α-SG is ecto-ATPase,[60] the reduced level of α-SG would result in preservation of higher ATP concentration in δ-SG-deficient BIO14.6 hamsters. Clearly, the mechanism of enhanced ATP release in dystrophic animals is an important issue to be addressed in future studies, together with identification of the involving P2 receptor species. Our pharmacological experiments demonstrated that suramin is as effective as cariporide in suppressing muscle degeneration. Simultaneous administration of suramin and cariporide exerted an additive beneficial effect on muscle dysgenesis in BIO14.6 hamsters (Figure 8, A–C), it is also possible that other pathways in addition to P2 receptors may be involved in activation of NHE.

Cariporide and suramin were reported to exert the beneficial effect *in vivo* on tissue injury at least partly through the anti-inflammatory effect.[61–63] For example, cariporide was reported to attenuate leukocyte-dependent inflammatory responses and subsequent tissue damage in myocardial ischemia/reperfusion injury.[61] Thus, it is possible that these chemicals may prevent muscle damage via reduction in leukocyte-mediated inflammation. However, in addition to protective effects *in vivo*, we observed that cariporide and suramin effectively blocked the CK efflux from BIO14.6 myotubes. This observation suggests that these chemicals can exert the protective effect by directly acting on skeletal muscles, although we do not exclude the possibility for their indirect beneficial effects *in vivo*.

In summary, we demonstrated that the NHE inhibitors cariporide and EIPA attenuate the muscle degeneration and myopathy in two dystrophic animal models, BIO14.6 hamsters and *mdx* mice. Based on detailed data obtained using cultured BIO14.6 myotubes, we propose that the activation of NHE is of primary importance in the pathogenesis of muscular dystrophy. We consider that P2 receptor activation by constantly released ATP would activate NHE and result in increases in $[Na^+]_i$, thereby increasing the resting level of $[Ca^{2+}]_i$ via NCX, together with activation of Ca^{2+} influx pathway TRPV2. However, it should be noted that protection by NHE inhibitors is not complete, which is reasonable in view of the underlying complexity of dystrophy. Nevertheless, our results suggest that, in principle, NHE inhibition represents a desirable approach to reduce muscle dysgenesis and may represent an attractive therapeutic approach. The benefits of NHE inhibitors could be accentuated when used in combination with other therapies for the treatment of muscular dystrophy. Although the underlying molecular mechanism is still unknown, our present study would provide a novel framework in signaling model connecting the genetic defect and muscle degeneration, which should be addressed in further studies.

Acknowledgments

We thank Dr. Munekazu Shigekawa (Senri Kinran University, Osaka, Japan) for initial participation and fruitful

discussion, and Ms. Ohtake for technical assistance in this study.

References

1. Duclos F, Straub V, Moore SA, Venzke DP, Hrstka RF, Crosbie RH, Durbeej M, Lebakken CS, Ettinger AJ, van der Meulen J, Holt KH, Lim LE, Sanes JR, Davidson BL, Faulkner JA, Williamson R, Campbell KP: Progressive muscular dystrophy in α-sarcoglycan-deficient mice. J Cell Biol 1998, 142:1461–1471
2. Campbell KP: Three muscular dystrophies: loss of cytoskeleton-extracellular matrix linkage. Cell 1995, 80:675–679
3. Nigro V, Okazaki Y, Belsito A, Piluso G, Matsuda Y, Politano L, Nigro G, Ventura C, Abbondanza C, Molinari AM, Acampora D, Nishimura M, Hayashizaki Y, Puca GA: Identification of the Syrian hamster cardiomyopathy gene. Hum Mol Genet 1997, 6:601–607
4. Campbell KP, Kahl SD: Association of dystrophin and an integral membrane glycoprotein. Nature 1989, 338:259–262
5. Tinsley JM, Blake DJ, Zuellig RA, Davies KE: Increasing complexity of the dystrophin-associated protein complex. Proc Natl Acad Sci USA 1994, 91:8307–8313
6. Ervasti JM, Campbell KP: A role for the dystrophin-glycoprotein complex as a transmembrane linker between laminin and actin. J Cell Biol 1993, 122:809–823
7. Mallouk N, Jacquemond V, Allard B: Elevated subsarcolemmal Ca^{2+} in mdx mouse skeletal muscle fibers detected with Ca^{2+}-activated K^+ channels. Proc Natl Acad Sci USA 2000, 97:4950–4955
8. Robert V, Massimino ML, Tosello V, Marsault R, Cantini M, Sorrentino V, Pozzan T: Alteration in calcium handling at the subcellular level in mdx myotubes. J Biol Chem 2001, 276:4647–4651
9. Fong PY, Turner PR, Denetclaw WF, Steinhardt RA: Increased activity of calcium leak channels in myotubes of Duchenne human and mdx mouse origin. Science 1990, 250:673–676
10. Iwata Y, Katanosaka Y, Arai Y, Komamura K, Miyatake K, Shigekawa M: A novel mechanism of myocyte degeneration involving the Ca^{2+}-permeable growth factor-regulated channel. J Cell Biol 2003, 161:957–967
11. Iwata Y, Katanosaka Y, Shijun Z, Kobayashi Y, Hanada H, Shigekawa M, Wakabayashi S: Protective effects of Ca^{2+} handling drugs against abnormal Ca^{2+} homeostasis and cell damage in myopathic skeletal muscle cells. Biochem Pharmacol 2005, 70:740–751
12. Wakabayashi S, Shigekawa M, Pouyssegur J: Molecular physiology of vertebrate Na^+/H^+ exchangers. Physiol Rev 1997, 77:51–74
13. Orlowski J, Grinstein S: Diversity of the mammalian sodium/proton exchanger SLC9 gene family. Pflugers Arch 2004, 447:549–565
14. Counillon L, Pouyssegur J: The expanding family of eucaryotic Na^+/H^+ exchangers. J Biol Chem 2000, 275:1–4
15. Karmazyn M, Gan XT, Humphreys RA, Yoshida H, Kusumoto K: The myocardial Na(+)-H(+) exchange: structure, regulation, and its role in heart disease. Circ Res 1999, 85:777–786
16. Xiao XH, Allen DG: Role of Na^+/H^+ exchanger during ischemia and preconditioning in the isolated rat heart. Circ Res 1999, 85:723–730
17. Imahashi K, Kusuoka H, Hashimoto K, Yoshioka J, Yamaguchi H, Nishimura T: Intracellular sodium accumulation during ischemia as the substrate for reperfusion injury. Circ Res 1999, 84:1401–1406
18. Tawada-Iwata Y, Imagawa T, Yoshida A, Takahashi M, Nakamura H, Shigekawa M: Increased mechanical extraction of T-tubule/junctional SR from cardiomyopathic hamster heart. Am J Physiol 1993, 264:H1447–H1453
19. Bertrand B, Wakabayashi S, Ikeda T, Pouyssegur J, Shigekawa M: The Na^+/H^+ exchanger isoform 1 (NHE1) is a novel member of the calmodulin-binding proteins. Identification and characterization of calmodulin-binding sites. J Biol Chem 1994, 269:13703–13709
20. Pang T, Su X, Wakabayashi S, Shigekawa M: Calcineurin homologous protein as an essential cofactor for Na^+/H^+ exchangers. J Biol Chem 2001, 276:17367–17372
21. Kusumoto K, Haist JV, Karmazyn M: Na^+/H^+ exchange inhibition reduces hypertrophy and heart failure after myocardial infarction in rats. Am J Physiol 2001, 280:H738–H745
22. Kharlamov A, Jones SC, Kim DK: Suramin reduces infarct volume in a model of focal brain ischemia in rats. Exp Brain Res 2002, 147:353–359
23. Iwata Y, Nakamura H, Mizuno Y, Yoshida M, Ozawa E, Shigekawa M: Defective association of dystrophin with sarcolemmal glycoproteins in the cardiomyopathic hamster heart. FEBS Lett 1993, 329:227–231
24. Iwata Y, Sampaolesi M, Shigekawa M, Wakabayashi S: Syntrophin is an actin-binding protein the cellular localization of which is regulated through cytoskeletal reorganization in skeletal muscle cells. Eur J Cell Biol 2004, 83:555–565
25. Bianchini L, L'Allemain G, Pouyssegur J: The p42/p44 mitogen-activated protein kinase cascade is determinant in mediating activation of the Na^+/H^+ exchanger (NHE1 isoform) in response to growth factors. J Biol Chem 1997, 272:271–279
26. Sabri A, Byron KL, Samarel AM, Bell J, Lucchesi PA: Hydrogen peroxide activates mitogen-activated protein kinases and Na^+-H^+ exchange in neonatal rat cardiac myocytes. Circ Res 1998, 82:1053–1062
27. Moor AN, Fliegel L: Protein kinase-mediated regulation of the Na^+/H^+ exchanger in the rat myocardium by mitogen-activated protein kinase-dependent pathways. J Biol Chem 1999, 274:22985–22992
28. Snabaitis AK, Yokoyama H, Avkiran M: Roles of mitogen-activated protein kinases and protein kinase C in alpha(1A)-adrenoceptor-mediated stimulation of the sarcolemmal Na^+-H^+ exchanger. Circ Res 2000, 86:214–220
29. Iwamoto T, Watano T, Shigekawa M: A novel isothiourea derivative selectively inhibits the reverse mode of $Na^+/Ca2^+$ exchange in cells expressing NCX1. J Biol Chem 1996, 271:22391–22397
30. Ryten M, Yang SY, Dunn PM, Goldspink G, Burnstock G: Purinoceptor expression in regenerating skeletal muscle in the mdx mouse model of muscular dystrophy and in satellite cell cultures. FASEB J 2004, 18:1404–1406
31. Yeung D, Zablocki K, Lien CF, Jiang T, Arkle S, Brutkowski W, Brown J, Lochmuller H, Simon J, Barnard EA, Gorecki DC: Increased susceptibility to ATP via alteration of P2X receptor function in dystrophic mdx mouse muscle cells. FASEB J 2006, 20:610–620
32. Dunn JF, Tracey I, Radda GK: A 31P-NMR study of muscle exercise metabolism in mdx mice: evidence for abnormal pH regulation. J Neurol Sci 1992, 113:108–113
33. Kumar A, Khandelwal N, Malya R, Reid MB, Boriek AM: Loss of dystrophin causes aberrant mechanotransduction in skeletal muscle fibers. FASEB J 2004, 18:102–113
34. Hnia K, Hugon G, Rivier F, Masmoudi A, Mercier J, Mornet D: Modulation of p38 mitogen-activated protein kinase cascade and metalloproteinase activity in diaphragm muscle in response to free radical scavenger administration in dystrophin-deficient Mdx mice. Am J Pathol 2007, 170:633–643
35. Dunn JF, Burton KA, Dauncey MJ: Ouabain sensitive Na^+/K^+-ATPase content is elevated in mdx mice: implications for the regulation of ions in dystrophic muscle. J Neurol Sci 1995, 133:11–15
36. Dunn JF, Bannister N, Kemp GJ, Publicover SJ: Sodium is elevated in mdx muscles: ionic interactions in dystrophic cells. J Neurol Sci 1993, 114:76–80
37. Yeung EW, Head SI, Allen DG: Gadolinium reduces short-term stretch-induced muscle damage in isolated mdx mouse muscle fibres. J Physiol 2003, 552:449–458
38. Alderton JM, Steinhardt RA: Calcium influx through calcium leak channels is responsible for the elevated levels of calcium-dependent proteolysis in dystrophic myotubes. J Biol Chem 2000, 275: 9452–9460
39. Nakamura TY, Iwata Y, Sampaolesi M, Hanada H, Saito N, Artman M, Coetzee WA, Shigekawa M: Stretch-activated cation channels in skeletal muscle myotubes from sarcoglycan-deficient hamsters. Am J Physiol 2001, 281:C690–C699
40. Gilbert JR, Meissner G: Sodium-calcium ion exchange in skeletal muscle sarcolemmal vesicles. J Membr Biol 1982, 69:77–84
41. Balnave CD, Allen DG: Evidence for $Na^+/Ca2^+$ exchange in intact single skeletal muscle fibers from the mouse. Am J Physiol 1998, 274:C940–C946
42. Geukes Foppen RJ, van Mil HG, van Heukelom JS: Effects of chloride transport on bistable behaviour of the membrane potential in mouse skeletal muscle. J Physiol 2002, 542:181–191
43. Bers DM, Ginsburg KS: Na:Ca stoichiometry and cytosolic Ca-dependent activation of NCX in intact cardiomyocytes. Ann NY Acad Sci 2007, 1099:326–338
44. Riedel MJ, Baczko I, Searle GJ, Webster N, Fercho M, Jones L, Lang J, Lytton J, Dyck JR, Light PE: Metabolic regulation of

sodium-calcium exchange by intracellular acyl CoAs. EMBO J 2006, 25:4605–4614
45. Carroll JE, Villadiego A, Brooke MH: Increased long chain acyl CoA in Duchenne muscular dystrophy. Neurology 1983, 33:1507–1510
46. Calaghan S, White E: Activation of Na^+-H^+ exchange and stretch-activated channels underlies the slow inotropic response to stretch in myocytes and muscle from the rat heart. J Physiol 2004, 559:205–214
47. Cingolani HE, Perez NG, Pieske B, von Lewinski D, Camilion de Hurtado MC: Stretch-elicited Na+/H+ exchanger activation: the autocrine/paracrine loop and its mechanical counterpart. Cardiovasc Res 2003, 57:953–960
48. North RA: Molecular physiology of P2X receptors. Physiol Rev 2002, 82:1013–1067
49. Fadic R: Cell surface and gene expression regulation molecules in dystrophinopathy: mdx vs. Duchenne. Biol Res 2005, 38:375–380
50. Perrone CE, Fenwick-Smith D, Vandenburgh HH: Collagen and stretch modulate autocrine secretion of insulin-like growth factor-1 and insulin-like growth factor binding proteins from differentiated skeletal muscle cells. J Biol Chem 1995, 270:2099–2106
51. Beigi R, Kobatake E, Aizawa M, Dubyak GR: Detection of local ATP release from activated platelets using cell surface-attached firefly luciferase. Am J Physiol 1999, 276:C267–C278
52. Pellegatti P, Falzoni S, Pinton P, Rizzuto R, Di Virgilio F: A novel recombinant plasma membrane-targeted luciferase reveals a new pathway for ATP secretion. Mol Biol Cell 2005, 16:3659–3665
53. Coco S, Calegari F, Pravettoni E, Pozzi D, Taverna E, Rosa P, Matteoli M, Verderio C: Storage and release of ATP from astrocytes in culture. J Biol Chem 2003, 278:1354–1362
54. Sabirov RZ, Dutta AK, Okada Y: Volume-dependent ATP-conductive large-conductance anion channel as a pathway for swelling-induced ATP release. J Gen Physiol 2001, 118:251–266
55. Aleu J, Martin-Satue M, Navarro P, Perez de Lara I, Bahima L, Marsal J, Solsona C: Release of ATP induced by hypertonic solutions in Xenopus oocytes. J Physiol 2003, 547:209–219
56. Cotrina ML, Lin JH, Alves-Rodrigues A, Liu S, Li J, Azmi-Ghadimi H, Kang J, Naus CC, Nedergaard M: Connexins regulate calcium signaling by controlling ATP release. Proc Natl Acad Sci USA 1998, 95:15735–15740
57. Stout CE, Costantin JL, Naus CC, Charles AC: Intercellular calcium signaling in astrocytes via ATP release through connexin hemichannels. J Biol Chem 2002, 277:10482–10488
58. Bodin P, Burnstock G: Purinergic signalling: ATP release. Neurochem Res 2001, 26:959–969
59. Roman RM, Wang Y, Lidofsky SD, Feranchak AP, Lomri N, Scharschmidt BF, Fitz JG: Hepatocellular ATP-binding cassette protein expression enhances ATP release and autocrine regulation of cell volume. J Biol Chem 1997, 272:21970–21976
60. Betto R, Senter L, Ceoldo S, Tarricone E, Biral D, Salviati G: Ecto-ATPase activity of alpha-sarcoglycan (adhalin). J Biol Chem 1999, 274:7907–7912
61. Redlin M, Werner J, Habazettl H, Griethe W, Kuppe H, Pries AR: Cariporide (HOE 642) attenuates leukocyte activation in ischemia and reperfusion. Anesth Analg 2001, 93:1472–1479
62. Németh ZH, Deitch EA, Lu Q, Szabo C, Hasko G: NHE blockade inhibits chemokine production and NF-κB activation in immunostimulated endothelial cells. Am J Physiol 2002, 283:C396–C403
63. Shiono T, Kodama M, Hanawa H, Fuse K, Yamamoto T, Aizawa Y: Suppression of myocardial inflammation using suramin, a growth factor blocker. Circ J 2002, 66:385–389

THE JOURNAL OF BIOLOGICAL CHEMISTRY VOL. 282, NO. 4, pp. 2741–2751, January 26, 2007

Solution Structure of the Cytoplasmic Region of Na^+/H^+ Exchanger 1 Complexed with Essential Cofactor Calcineurin B Homologous Protein 1*[S]

Received for publication, April 28, 2006, and in revised form, October 6, 2006 Published, JBC Papers in Press, October 18, 2006, DOI 10.1074/jbc.M604092200

Masaki Mishima[‡], Shigeo Wakabayashi[§], and Chojiro Kojima[‡1]

From the [‡]Graduate School of Biological Sciences, Nara Institute of Science and Technology, Ikoma, Nara 630-0192, Japan and [§]Department of Molecular Physiology, National Cardiovascular Center Research Institute, Suita, Osaka 565-8565, Japan

Na^+/H^+ exchanger 1 (NHE1) regulates intracellular pH, Na^+ content, and cell volume. Calcineurin B homologous protein 1 (CHP1) serves as an essential cofactor that facilitates NHE1 exchange activity under physiological conditions by direct binding to the cytoplasmic juxtamembrane region of NHE1. Here we describe the solution structure of the cytoplasmic juxtamembrane region of NHE1 complexed with CHP1. The region of NHE1 forms an amphipathic helix, which is induced by CHP1 binding, and CHP1 possesses a large hydrophobic cleft formed by EF-hand helices. The apolar side of the NHE1 helix participates in extensive hydrophobic interactions with the cleft of CHP1. We suggest that helix formation of the cytoplasmic region of NHE1 by CHP1 is a prerequisite for generating the active form of NHE1. The molecular recognition detailed in this study also provides novel insight into the target binding mechanism of EF-hand proteins.

Na^+/H^+ exchangers comprise a family of countertransport proteins that catalyze the electroneutral exchange of Na^+ and H^+. Nine isoforms of the Na^+/H^+ exchanger have been isolated and shown to possess similar membrane topologies consisting of 12 N-terminal membrane-spanning helices and a large C-terminal cytoplasmic region (Fig. 1*A*). The exchanger isoforms exhibit tissue-specific expression, membrane localization, and kinetic and pharmacological properties (1). They participate in a broad range of physiological processes including the regulation of cell volume, transepithelial transport of electrolytes, cell proliferation, apoptosis, and differentiation. Isoforms NHE1–5, localized at the plasma membrane, are primarily involved in the regulation of intracellular pH (pH_i)[2] and Na^+ concentration (1).

Of them, the ubiquitously expressed isoform NHE1 is the best studied mammalian Na^+/H^+ exchanger. The activity is controlled by various extrinsic factors including hormones, growth factors, pharmacological agents, and mechanical stimuli (1). The regulation of NHE1 by these external stimuli is thought to be exerted through the action of a variety of signaling molecules including calcineurin B homologous protein (2, 3), calmodulin (4, 5), low molecular mass GTPases of the Ras and Rho family (6–8), p42/44 mitogen-activated protein kinases (9), p90 ribosomal S6 kinase (10), 14-3-3 protein (11), Nck-interacting kinase (12), and phosphatidylinositol 4,5-bisphosphate (13). However, the detailed mechanism through which these events occur remains unknown.

Among these factors, CHP1 can serve as an essential cofactor and is required by at least three NHE isoforms (NHE1–3) to express high physiological levels of exchange activity (3). It was shown that CHP1 bound directly to the juxtamembrane region of the C-terminal cytoplasmic domain. When GFP-CHP1 and NHE1–3 were co-expressed, it was found that GFP-CHP1 was mostly localized at the cell surface, whereas co-expression of CHP1 and a CHP1 binding-defective NHE1 mutant failed to show co-localization, implying that NHE1 is a principal target of CHP1 (3). In addition to reduced activity in the neutral pH range, the CHP1 binding-defective NHE1 mutant showed a marked reduction in pH_i sensitivity (~0.7 pH unit acidic shift) that subsequently abolished various NHE1 regulatory responses. Furthermore CHP1 deprivation resulted in marked reduction (>90%) of NHE1 activity (3). These observations suggest that the association of NHE1 with CHP1 is critical for activity and the maintenance of NHE1 pH_i sensitivity (14).

CHP1 consists of four EF-hands, the primary sequence of which is homologous to calmodulin (CaM) and calcineurin B

* This work was supported in part by grants-in-aid for Scientific Research on Priority Area and the 21st Century of Excellence (COE) Program from the Ministry of Education, Culture, Sports, Science and Technology (MEXT), Japan (to M. M. and C. K.), and Grant nano-001 for Research on Advanced Medical Technology from the Ministry of Health, Labor and Welfare of Japan and Grant-in-aid for Priority Areas 13142210 for Scientific Research from the MEXT (to S. W.). The costs of publication of this article were defrayed in part by the payment of page charges. This article must therefore be hereby marked "*advertisement*" in accordance with 18 U.S.C. Section 1734 solely to indicate this fact.

[S] The on-line version of this article (available at http://www.jbc.org) contains supplemental Table S1 and Figs. S2 and S3.

The atomic coordinates and structure factors (code 2E30) have been deposited in the Protein Data Bank, Research Collaboratory for Structural Bioinformatics, Rutgers University, New Brunswick, NJ (http://www.rcsb.org/).

[1] To whom correspondence should be addressed: Graduate School of Biological Sciences, Nara Institute of Science and Technology, 8916-5 Takayama, Ikoma, Nara 630-0192, Japan. Tel.: 81-743-72-5571; Fax: 81-743-72-5579; E-mail: kojima@bs.naist.jp.

[2] The abbreviations used are: pH_i, intracellular pH; HSQC, heteronuclear single quantum coherence; NOE, nuclear Overhauser effect; NOESY, NOE spectroscopy; TOCSY, total correlation spectroscopy; CANDID, combined automated NOE assignment and structure determination module; CaM, calmodulin; CNB, calcineurin B; NHE, Na^+/H^+ exchanger; CHP, calcineurin B homologous protein; CNA, calcineurin A; Ni-NTA, nickel-nitrilotriacetic acid; GST, glutathione *S*-transferase; CHAPS, 3-[(3-cholamidopropyl)dimethylammonio]-1-propanesulfonic acid; r.m.s., root mean square; Kv, voltage-gated potassium channel; KChIP, Kv-interacting protein; PIP_2, phosphatidylinositol 4,5-bisphosphate.

Supplemental Material can be found at: http://www.jbc.org/cgi/content/full/M604092200/DC1

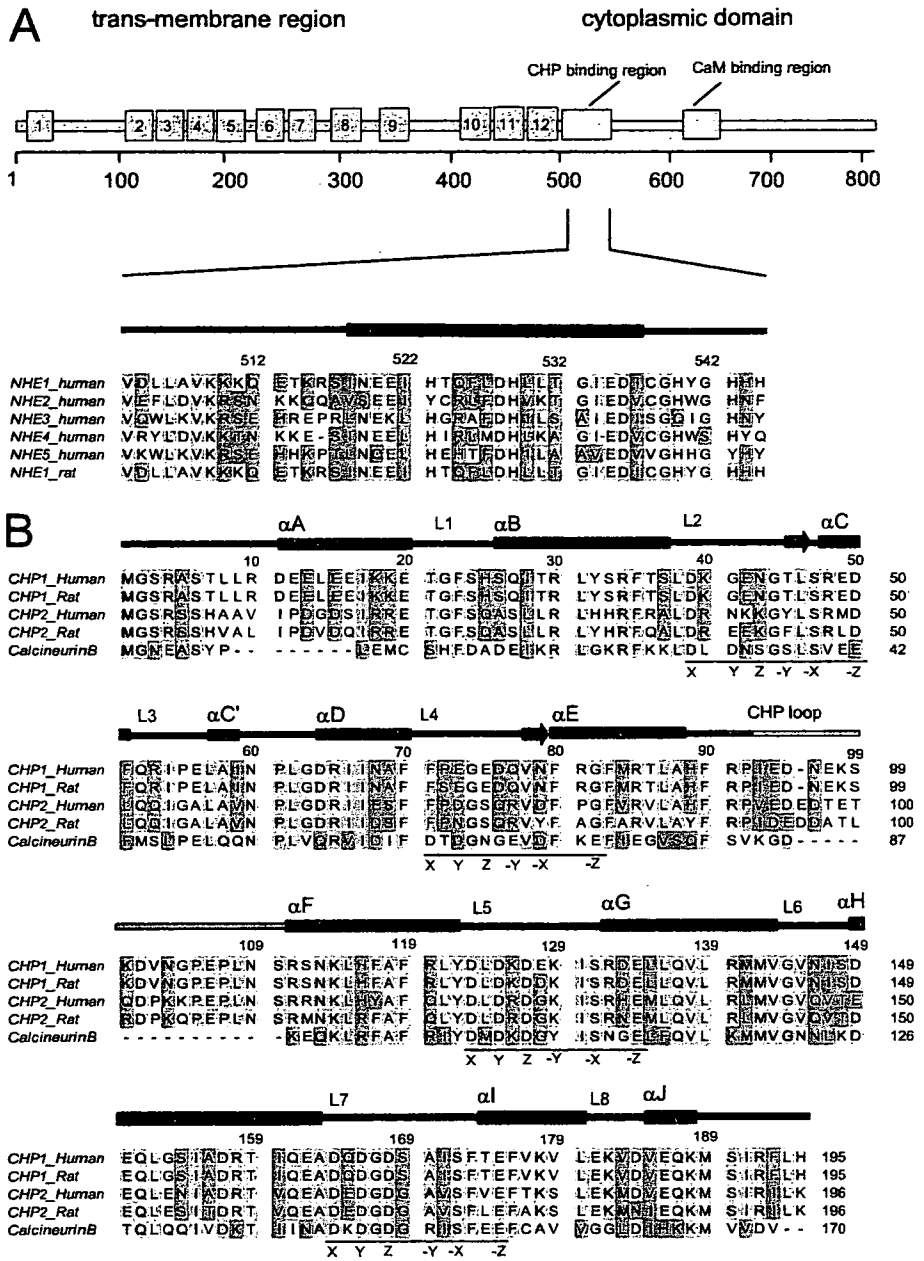

FIGURE 1. **Multiple sequence alignments of NHE1 and CHP1.** *A*, domain structure and alignment of NHE1. *B*, alignment of CHP1, CHP2, and human calcineurin B. In *A* and *B*, sequence alignment was performed using ClustalW. Secondary structure elements of the proteins are shown schematically at the *top* of the alignments. N- and C-terminal domains of CHP1 are colored in *blue* and *magenta*, respectively, for clarity. Conserved and semiconserved residues are colored in *yellow* and *green*, respectively. The 12-residue motif involved in the EF-hand is *underlined*, and key residues are indicated as *X*, *Y*, *Z*, *-Y*, *-X*, and *-Z*.

(CNB), possessing 31 and 41% sequence identity, respectively (Fig. 1*B*). It is well known that all CaM and CNB EF-hands can bind Ca^{2+}. However, CHP1 EF-1 and EF-2 are ancestral and do not bind Ca^{2+} under physiological conditions, whereas EF-3 and EF-4 bind two Ca^{2+} ions with high affinity (~90 nM) based on the $^{45}Ca^{2+}$ binding experiments for several CHP1 mutants (14). Complex formation between CHP1 and the CHP1 binding domain of NHE1 resulted in a marked increase in Ca^{2+} binding affinity (K_d = ~2 nM) (14). This suggests that CHP1 constitutively contains two Ca^{2+} ions when associated with NHE1 in cells (14).

Interestingly CHP1 has been reported to exhibit multiple functions. It was initially identified as a protein (p22) involved in vesicular transport (15) and the inhibition of calcineurin phosphatase activity (16). It was also found to interact with microtubules (17), DRAK2 (death-associated protein kinase-related apoptosis-inducing protein kinase 2) (18) and KIF1Bβ2 (kinesin family 1Bβ2) (19).

A second CHP isoform, CHP2, with 61% sequence identity was also identified and found to be involved in the maintenance of abnormally high pH_i in malignantly transformed cells. CHP2 is expressed at a relatively high level in malignantly transformed cells and in rat small intestine, suggesting that it plays a specific role in this tissue (20). In addition, tescalcin, an EF-hand protein closely related to CNB, that interacts with the cytoplasmic region of NHE1 has been identified (21, 22).

The crystal structure of NHE1-unbound rat CHP1 was recently determined and revealed that the overall structure is similar to CNB where Ca^{2+} ions are coordinated within EF-3 and EF-4. However, the interaction mechanism between NHE1 and CHP1 remains unknown (23).

Here we report on the solution structure of the cytoplasmic region of NHE1 bound to CHP1 as determined by NMR. Details of the NHE1-CHP1 interaction are described. We present mutational binding data to delineate the significance of the interactions observed in the complex. Based on the structure, we suggest a role for CHP1 in terms of NHE1 activation. Comparisons of the binding mode between NHE1-CHP1 and calcineurin A (CNA), CNB, and other related four-EF-hand proteins are also discussed.

EXPERIMENTAL PROCEDURES

Sample Preparation—The NHE1-CHP1 complex was co-expressed and co-purified. DNA encoding NHE1 was cloned into the pET24a vector (Novagen), and CHP1 was subcloned into pET11a (Novagen), which produces recombinant protein with a hexahistidine (His_6) sequence at the C terminus. The proteins were co-overexpressed in *Escherichia coli* BL21(DE3) cells. Uniformly ^{15}N- and $^{15}N/^{13}C$-labeled proteins were prepared by

growing bacteria in minimal medium containing $^{15}NH_4Cl$ with or without [$^{13}C_6$]glucose. Uniformly $^{15}N/^{13}C$-labeled and fractionally deuterated protein sample was prepared using medium containing 60% ^2H_2O. The NHE1-CHP1 complex was purified using a standard Ni-NTA affinity column protocol (Qiagen). Further purification was performed by gel filtration using Superdex 200 (GE Healthcare). NMR samples contained 0.5–0.9 mM protein in 50 mM Tris-d_7 buffer (pH 6.9), 1 mM dithiothreitol-d_{10}, 30 mM KCl in $H_2O/^2H_2O$ (9:1) or ^2H_2O.

NMR Spectroscopy—NMR data were recorded at 37 °C on Bruker AVANCE 500 and DRX 800 NMR spectrometers. Resonance assignments for ^{1}HN, ^{15}N, $^{13}C\alpha$, $^{13}C\beta$, and $^{13}C'$ nuclei for the CHP1-NHE1 complex were obtained through the following ^{2}H-decoupled, triple resonance spectra applied to a fractionally deuterated $^{15}N/^{13}C$-labeled sample: three-dimensional HNCACB/HN(CO)CACB (24) and three-dimensional HN(CA)CO/HNCO experiments (25, 26). Side-chain ^{1}H and ^{13}C resonances were assigned on a fully protonated sample or a fractionally deuterated $^{15}N/^{13}C$-labeled sample using three-dimensional C(CO)NH, three-dimensional H(CCO)NH, four-dimensional HC(CO)NH, and three-dimensional HCCH TOCSY (27–29). Stereospecific assignment of leucine and valine methyl groups were obtained from a Constant Time-$^1H/^{13}C$ HSQC spectrum of a 15% ^{13}C-labeled sample (30). $^1H\alpha$ and $^1H\beta$ resonance assignments were supplemented with three-dimensional H(CACO)NH (31), ^{15}N-edited TOCSY-HSQC (32), and three-dimensional HBHA(CBCACO)NH (33). Aromatic resonances of both NHE1 and CHP1 were mainly assigned using three-dimensional ^{13}C-aromatic-edited/^{15}N-separated NOESY-HSQC, three-dimensional ^{13}C-edited NOESY, ^1H-^1H TOCSY, and NOESY experiments (32). The assignment was verified using the Constant Time-$^1H/^{13}C$ HSQC spectrum of a 15% ^{13}C-labeled sample (30). The following NOESY spectra were recorded for the protonated sample and used to generate distance restraints for structure calculations: three-dimensional ^{15}N-edited NOESY (80-ms mixing time), three-dimensional ^{13}C-edited NOESY (80-ms mixing time), and two-dimensional ^{1}H NOESY (80-ms mixing time). Slowly exchanging amide protons were identified from a series of two-dimensional ^{15}N HSQC spectra recorded after the H_2O buffer was replaced with ^2H_2O buffer. All NMR spectra were processed using NMRPipe/NMRDraw (34) analyzed using SPARKY (35).

Structure Calculations—Intramolecular and intermolecular distance constraints were identified in the three-dimensional $^{15}N/^{13}C$-separated NOESY spectra using a $^{15}N/^{13}C$-labeled NHE1-CHP sample with mixing times of 80 ms. Backbone hydrogen bond restraints within regular secondary structure elements that were consistent with backbone amide hydrogen/deuterium exchange data were included in the structure calculations. The initial structure calculations were performed by iterative automated assignment of the NOE spectra using CANDID (36) in addition to manually assigned NOE-derived distance restraints. The restraints, leading to converged structures, were subsequently utilized for the iterative automated assignment of all spectra including aromatic residues using CANDID. Finally refinement of the structures (including two Ca^{2+} ions) using XPLOR-NIH (version 2.96) was performed (37). The final structure calculations used a total of 4022 NOE-derived distance restraints obtained from the manual and the CANDID-assisted assignments from the ^{15}N- or ^{13}C-edited NOE data. A total of 100 simulated annealing structures were calculated, and 20 structures were selected that possessed no NOE violations greater than 0.5 Å and no dihedral violations greater than 5°. Final structures were evaluated using the program ProcheckNMR (38). Structures and figures were drawn using MOLMOL (39), GRASP (40), and Chimera (41).

Mutagenesis and GST Pulldown Assay—For the binding analyses, CHP1 was expressed as a fusion protein with GST in *E. coli*, which was then subcloned into modified pGEX6P-3 (Novagen) (42). Site-directed mutant proteins were prepared using the QuikChange kit (Stratagene). DNA sequencing confirmed the mutations. Vectors were transformed into BL21(DE3)star (Invitrogen). Cells were grown at 37 °C and then induced with 1 mM isopropyl 1-thio-β-D-galactopyranoside for 12 h at 20 °C. Harvested cells were disrupted via sonication in HEPES (pH 8.0) containing 10% glycerol, 10% sucrose, 1 mM dithiothreitol, and 30 mM KCl. The GST-CHP1 fusion protein was purified using glutathione-Sepharose (GE Healthcare) and a standard protocol except that the equilibrium buffer was changed to 50 mM HEPES buffer (pH 8.0) containing 10% glycerol, 1 mM dithiothreitol, and 30 mM KCl, and the column was washed extensively with 20 mM CHAPS. The effect of mutation on the binding of CHP1 to NHE1 peptides was characterized using a GST pulldown assay. Synthetic NHE1 peptide (residues 514–545 including a hexahistidine sequence at the C terminus) was purchased from Greiner Japan (Tokyo, Japan). Briefly wild-type and CHP1 mutant GST fusion proteins, in addition to GST alone, were incubated for 30 min at 20 °C with NHE1 peptide in binding buffer containing 50 mM HEPES (pH 7.5), 20 mM CHAPS, 10% glycerol, 1 mM Pefabloc, and 1 mM dithiothreitol. GST protein-bound Sepharose beads were washed extensively with binding buffer. Proteins were resolved by 12% NuPAGE (Invitrogen) and blotted onto membranes, and then His-NHE1 was analyzed with Ni-NTA-conjugated alkaline phosphatase (Promega) and Western Blue substrate (Promega). Quantification was represented as the average value of experiments performed in triplicate.

RESULTS AND DISCUSSION

Structure Determination—To better understand the mechanism pertaining to CHP1-regulated NHE1 activity, the solution structure of unmyristoylated CHP1 complexed with the cytoplasmic region (503–545) of NHE1 was determined by NMR spectroscopy. Our structural studies were initially hampered by the fact that NHE1-free CHP1 tended to aggregate during NMR measurements, and the CHP1-unbound cytoplasmic region (503–545) of NHE1 readily degraded during the expression and purification steps. Consequently NMR structural analysis of co-expressed and co-purified samples was undertaken. Co-expression of CHP1 and NHE1-(503–545) produced a stable complex for structural studies and showed no significant degradation and aggregation for several weeks.

The ^1H-^{15}N HSQC spectrum of NHE1-unbound CHP1 displays many broadened peaks presumably due to formation of a dimer, multimer, or an equilibrium between these states in solution. In contrast, the HSQC spectrum of ^{15}N-labeled CHP1

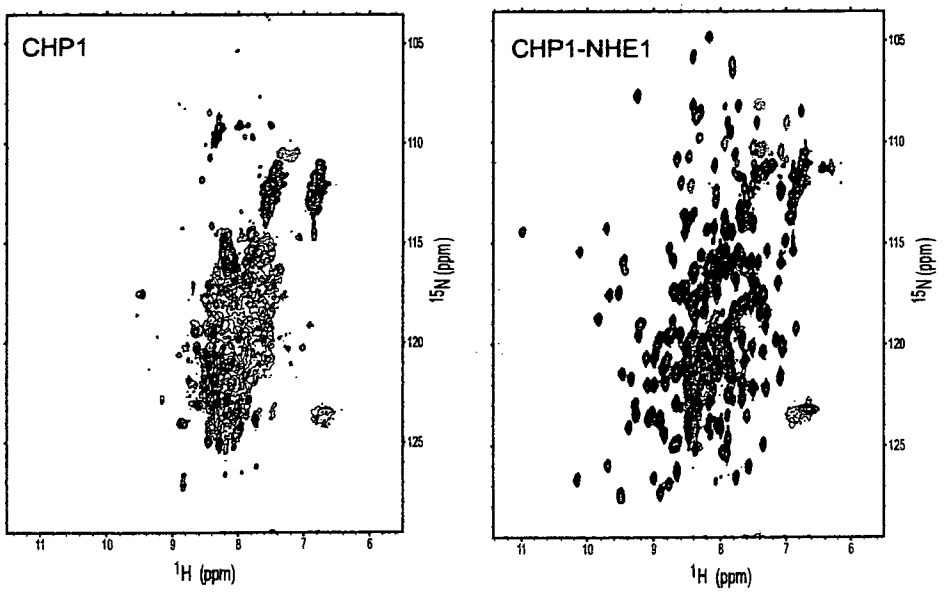

FIGURE 2. **^{1}H-^{15}N HSQC spectra of ^{15}N-labeled NHE1-free CHP1 (*left image*) and ^{15}N-labeled NHE1-(503–545)-CHP1 complex (*right image*).** These spectra were obtained with 0.3 mM samples at pH 6.9 and 37 °C recorded on the AVANCE 500.

TABLE 1

Structural statistics for NHE1-CHP1

These statistics represent an ensemble comprising 20 of the lowest energy structures obtained from 150 starting structures. Structure calculations were performed using XPLOR-NIH version 2.9.6.

Total number of distance constraints	4242
Long range ($\|i-j\|>4$)	589 (inter: 134)
Middle range ($\|i-j\|=2,3,4$)	874
Short range ($\|i-j\|=1$)	1038
Intraresidue	1521
Hydrogen bond constraints (including Ca^{2+} coordination restraints)	110 × 2
Dihedral constraints	
ϕ, φ	105, 105
$\chi 1$	17
r.m.s. deviation from experimental constraints[a]	
Distance (Å)	$0.0288 \pm 7 \times 10^{-4}$
Angle (°)	$0.44 \pm 3 \times 10^{-2}$
r.m.s. deviation from idealized covalent geometry	
Bonds (Å)	$0.00248 \pm 6 \times 10^{-5}$
Angles (°)	$0.360 \pm 6 \times 10^{-3}$
Impropers (°)	$0.31 \pm 1 \times 10^{-2}$
XPLOR energy terms (kcal/mol)[b]	
E_{bond}	23 ± 1
E_{angle}	138 ± 5
E_{imp}	28 ± 2
$E_{vdw(LJ)}$	$-6.6 \times 10^{2} \pm 0.2 \times 10^{2}$
PROCHECK Ramachandran plot (185–254)	
Residues in most favored regions (%)	78.6
Residues in additional allowed regions (%)	18.1
Residues in generously allowed regions (%)	2.9
Residues in disallowed regions (%)	0.4
r.m.s. deviation of mean structure derived from 30 calculated structures	
Backbone (10–92, 108–192, 516–538) (Å)	0.53
All heavy (10–92, 108–192, 516–538) (Å)	1.15

[a] None of these structures exhibited distance violations >0.5 or dihedral angle violations >5°.

[b] $E_{vdw(LJ)}$ represents the Lennard-Jones energy of the XPLOR energy terms.

complexed with NHE1 is well dispersed with favorable line shapes (Fig. 2), suggesting that the complex essentially adopts an ordered monomeric structure in solution.

Our target complex was ~27 kDa in size, assuming a 1:1 complex of CHP1 (22 kDa) and NHE1 (5 kDa). This represented a relatively large molecular weight in terms of conventional NMR studies. Consequently utilization of triple labeling (^{2}H, ^{13}C, and ^{15}N) and the recently developed computational methodology, CANDID, was extremely helpful in the structure determination. Sequential backbone assignments and most side-chain assignments were obtained from a 60% ^{2}H/^{15}N/^{13}C-labeled sample using standard triple resonance experiments. Missing ^{1}H resonances were supplemented using heteronuclear three-dimensional NOESY experiments with ^{15}N/^{13}C-labeled samples. Resonance assignments of methyl groups were carefully confirmed in a stereospecific manner using two-dimensional Constant Time HSQC spectra recorded for a 15% randomly enriched ^{13}C sample. Methyl groups for 18 of 24 leucines and nine of 11 valines were stereospecifically assigned. Aromatic ring proton assignments, essential for delineating hydrophobic core and protein-protein interactions, were obtained using two-dimensional TOCSY, two-dimensional NOESY, two-dimensional HCCH(arom) TOCSY, and three-dimensional ^{13}C(arom)-edited ^{15}N-separated NOESY experiments.

NMR spectra including the three-dimensional ^{13}C-edited NOESY spectrum used to monitor inter/intramolecular ^{1}H-^{1}H NOEs were of adequate quality to pursue a structural determination of the NHE1-CHP1 complex. Use of partial deuteration and the almost complete resonance assignment of methyl groups forming the hydrophobic core facilitated an initial determination of the overall protein fold. A high resolution structure was subsequently obtained using CANDID for automated assignments, which included the use of ambiguous NOEs from ^{15}N- and ^{13}C-edited NOESY experiments recorded for ^{15}N- or ^{15}N/^{13}C-labeled protein samples. An iterative approach was used for assigning NOEs in addition to the manually assigned unambiguous NOEs. The solution structure of the CHP1-NHE1 complex was determined from a total of over 4000 NMR-derived restraints, including 134 intermolecular distance restraints (Table 1). The ensemble of 20 structures in excellent agreement with a large body of experimental data were well defined (Fig. 3*A*). The r.m.s. deviations of backbone and heavy atoms over residues 518–537 of NHE1 and residues 10–92 and 108–193 of CHP1 were 0.53 and 1.15 Å, respectively. Of the NMR structures determined, the one with the smallest total energy was selected as representative for further discussion. The complex is predominantly α-helical, and the CHP1 helices constitute a cleft. A helix of the cytoplasmic region of NHE1 associates with CHP1 in 1:1 stoichiometry via the cleft (Fig. 3, *A* and *B*).

Structure of NHE1—NHE1 forms a five-turn amphipathic helix composed of residues 518–537. Orientation of the NHE1 helix is well defined relative to CHP1, consistent with the large

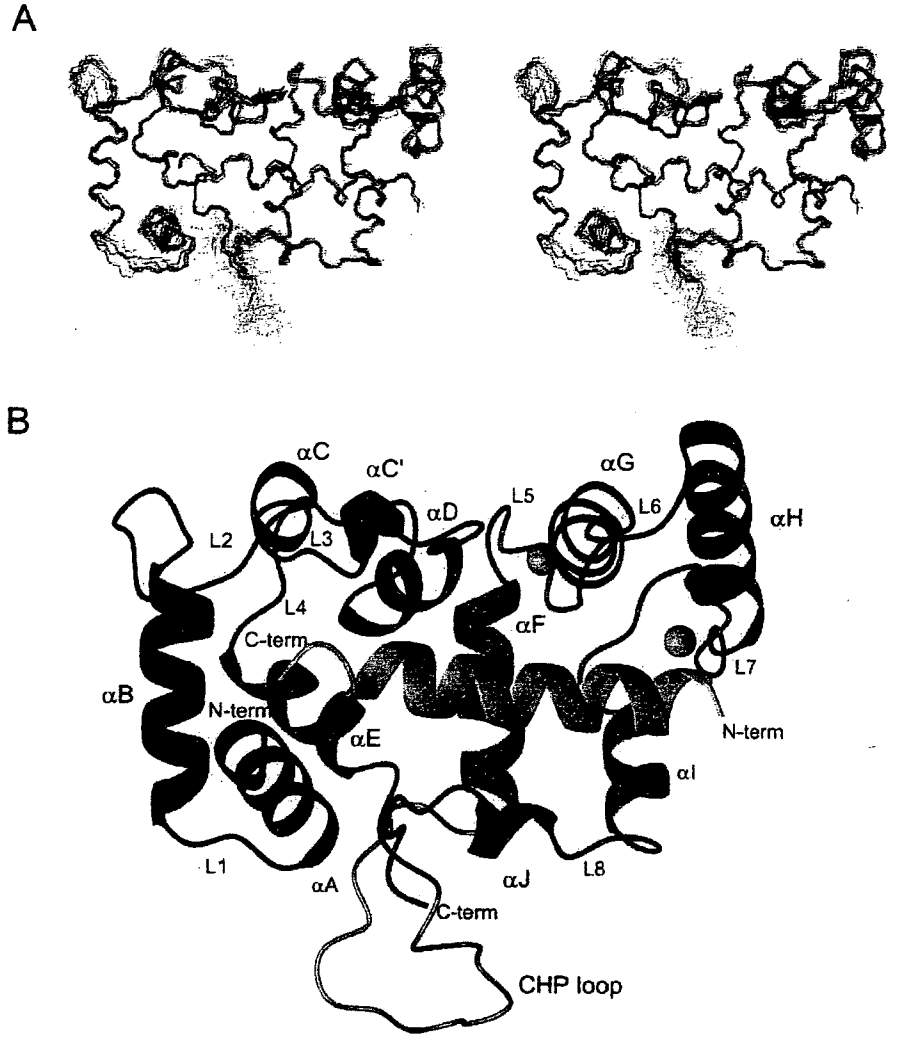

FIGURE 3. **Solution structure of the NHE1-CHP1 complex.** *A*, stereoview of the backbone superpositions of the final 20 simulated annealing structures of the NHE1-CHP1 complex. *B*, ribbon drawing of the representative NHE1-CHP1 structure complex. *A* and *B*, residues 517–538 of NHE1 and 10–192 of CHP1 are shown. The N- and C-terminal domains of CHP1 are colored in *blue* and *magenta*, respectively, and the CHP loop is colored in *gray*. NHE1 is shown in *green*. Ca^{2+} ions are shown by *gold spheres*.

number of intermolecular NOEs detected between CHP1 and NHE1 (Table 1 and Fig. 3*A*). The N-terminal half of the helix (residues 518–530) binds to the C-terminal domain of CHP1, and the C-terminal half of the helix (residues 531–537) binds to the N-terminal domain of CHP1 (Fig. 4*A*). Side-chain conformations of the helix are also well defined particularly for apolar residues that make extensive contacts with CHP1. For example, NMR spin-echo difference $^3J_{NC\gamma}$ and $^3J_{C'C\gamma}$ experiments, which bring about $\chi 1$ rotamer information of aromatic side chain, showed that the His-523 and Phe-526 adopted *g*+ and *t* conformations, respectively. The helix exhibits amphipathic character in which the bulky hydrophobic residues Ile-518, Ile-522, His-523, Phe-526, Leu-527, Leu-530, Leu-531, Ile-534, and Ile-537 are clearly confined to one side, and hydrophilic residues are exposed at the other side (Fig. 4*B*). The hydrophobic residues form a continuous apolar surface (Fig. 4*B*). The main-chain and side-chain conformations of residues preceding and following the helix, residues 503–517 and 538–545, respectively, are poorly defined in the NMR structure because of the absence of medium and long range NOEs involving these regions. The narrow resonance linewidths, chemical shift index, and steady state $\{^1H\}$-^{15}N heteronuclear NOE suggest that these regions are unstructured in the complex.

Structure of CHP1—CHP1 is composed of 10 α-helices and a long loop folded into two globular regions representing the N- and C-terminal domains (Fig. 3*B*). The secondary structure consists of αA (residues 11–22), αB (residues 26–37), αC (residues 48–51), αD (residues 64–70), αE (residues 80–88), αF (residues 111–122), αG (residues 132–143), αH (residues 149–162), αI (residues 174–180), and αJ (residues 185–188) (Figs. 1*B* and 3*B*). The N-terminal domain consists of ancestral EF-hands, EF-1 and EF-2, that do not bind calcium under physiological conditions. The EF-1 hand includes helix αB, loop L2, and helix αC followed by loop L3 to the second EF-hand that includes helix αD, loop L4, and helix αE (Figs. 1*B* and 3*B*). A long loop region consisting of residues 93–110 connects the N- and C-terminal domains. Because this characteristic long insertion is not found in calcineurin B (Figs. 1*B* and 3, *A* and *B*), we refer to this long loop as the CHP loop. The absence of medium and long range NOEs, a chemical shift index, and $\{^1H\}$-^{15}N heteronuclear NOE value indicate that this region is flexible in solution. The first EF-hand in the C-terminal domain includes helix αF, loop L5, and helix αG followed by loop L6 and the second EF-hand that consists of helix αH, loop L7, and helix αI (Figs. 1*B* and 3*B*).

The four CHP1 EF-hands form a deep hydrophobic pocket, which constitutes the interaction surface for the NHE1 amphipathic α-helix. CHP1 binds to the apolar side of NHE1 with the four EF-hands through a side-by-side manner (Fig. 4*A*). This contrasts with the well known canonical CaM-target binding mode that represents a wrap-around manner in which two pairs of EF-hands bind to the target IQ motif helix on opposite sides to each other (43, 44).

Although there is modest sequence similarity between CHP1 and CaM, it should be noted that the latter interacts with a large number of proteins with various interaction modes including canonical 1:1 binding and non-canonical 1:1, 1:2, and 2:2 binding (43, 44). It has been suggested that the observed binding versatility of CaM could be derived from the variable positioning of the two domains, linked by a flexible linker, that can